| RESEARCH ARTICLE OPEN ACCESS

A Dryopithecine Talus From Abocador de Can Mata (Vallès-Penedès Basin, NE Iberian Peninsula): Morphometric Affinities and Evolutionary Implications for Hominoid Locomotion

Oriol Monclús-Gonzalo[1] 🆔 | Shubham Pal[1] | Thomas A. Püschel[2] | Alessandro Urciuoli[1,3,4] | Víctor Vinuesa[1] | Josep M. Robles[1] | Sergio Almécija[1,5,6] | David M. Alba[1] 🆔

[1]Institut Català de Paleontologia Miquel Crusafont (ICP-CERCA), Universitat Autònoma de Barcelona, Barcelona, Spain | [2]Institute of Human Sciences, School of Anthropology, University of Oxford, Oxford, UK | [3]Department of Paleontology, University of Zurich, Zurich, Switzerland | [4]Departamento de Ciencias de la Vida, Universidad de Alcalá, Cátedra de Otoacústica Evolutiva y Paleoantropología (HM Hospitales-UAH), Madrid, Spain | [5]Division of Anthropology, American Museum of Natural History, New York, New York, USA | [6]New York Consortium in Evolutionary Primatology, New York, New York, USA

Correspondence: Oriol Monclús-Gonzalo (oriol.monclus@icp.cat) | David M. Alba (david.alba@icp.cat)

ABSTRACT

Objectives: The functional interpretation of postcranial remains of Middle Miocene great apes from Europe (dryopithecines) suggests a combination of quadrupedalism and orthograde behaviors without modern analogs. We provide further insights based on an isolated dryopithecine talus (IPS85037) from the Middle Miocene (11.7 Ma) Abocador de Can Mata locality ACM/C8-B* (Vallès-Penedès Basin, NE Iberian Peninsula), which represents the most complete one known to date.

Material and Methods: We compare the specimen with an extant anthropoid sample (n = 68) and the stem hominoid *Ekembo heseloni* (KMN RU 2036, ~18 Ma, Kenya) using 3D geometric morphometrics. For the two fossil tali, we assess their phenetic affinities using a between-group principal components analysis (bgPCA), estimate body mass based on centroid size, and make locomotor inferences using a partial least-squares regression (PLSR) between talar shape and locomotor repertoire.

Results: Its large inferred body mass (~38 kg) and the possession of several modern hominoid-like features (albeit combined with more plesiomorphic traits) support the attribution of IPS85037 to a male dryopithecine. The bgPCA indicates that IPS85037 falls close to the extant hominoid variation and is less cercopithecoid-like than that of *Ekembo*, whose inferred locomotor repertoire is vastly dominated by quadrupedalism (81%). In contrast, the locomotor repertoire inferred from IPS85037 combines important quadrupedal (32%) and vertical climbing/clambering (50%) components with only moderate suspension (10%).

Discussion: Our results align with previous inferences derived from other postcranial elements of Middle Miocene dryopithecines and, given their classification as crown hominoids, support the hypothesis that certain suspensory adaptations shared by extant hylobatids and hominids likely evolved independently.

1 | Introduction

1.1 | The Talus of Miocene Apes

The talus plays an important role in primate posture and locomotion, being involved in body weight transmission and stability/mobility at the ankle joint—including foot flexion-extension and abduction-adduction at the talocrural joint, pronation-supination at the subtalar joint, and flexion-extension at the midtarsal joint (Lewis 1980a, 1980b). Accordingly, talar morphology is tightly linked to foot function and substrate preference (Turley and Frost 2013; Parr et al. 2014), and these differences can even be characterized among closely related taxa (Dunn et al. 2014; Knigge et al. 2015; Friesen et al. 2024). Hence, the talus is of great value for making locomotor inferences in extinct primates (e.g., Day and Wood 1968, 1969; Lisowski et al. 1974, 1976; Alba et al. 2014; Marigó et al. 2016; Püschel et al. 2017; Püschel et al. 2018; Püschel et al. 2020).

Among hominoids (the ape and human clade), much emphasis has been devoted to the interpretation of talar morphology in fossil hominins in relation to bipedal adaptations (e.g., Day and Wood 1968; Latimer et al. 1987; Parr et al. 2014; Sorrentino et al. 2020). For Miocene apes, talar morphology has been mostly related to different types of arboreal behaviors, including the distinction between plesiomorphic (i.e., "monkey-like") quadrupedalism and more apomorphic (i.e., modern "ape-like") behaviors such as vertical climbing, suspension, and knuckle-walking (Day and Wood 1969; Lisowski et al. 1974, 1976; Langdon 1986). However, further insight into the evolution of talar morphology in extant hominoid lineages is hampered by the scarcity of fossil tali attributable to crown members of this group. On the other hand, there is a relatively good record of fossil tali of both putative stem catarrhines (Le Gros Clark and Thomas 1951; Harrison 1982; Morbeck 1983; Begun 1987; Leakey and Leakey 1987; Rose et al. 1992; Kordos and Begun 2001) and hominoids (Le Gros Clark and Leakey 1951; Le Gros Clark 1952; Harrison 1982; Walker and Pickford 1983; Hill and Ward 1988; Leakey et al. 1988; Ward et al. 1993; McCrossin 1994; Rose et al. 1996; Ward 1998; Ishida et al. 2004; Dunsworth 2006; Nakatsukasa et al. 2012; Russo et al. 2024) from the Early to Middle Miocene of Africa. In the Miocene of Eurasia, ape tali are more scarce, being restricted to the great apes (hominids) from the Late Miocene—one talus attributed to *Sivapithecus* (Pilbeam et al. 1977; Pilbeam et al. 1980; Morbeck 1983; Madar 1996) and an undescribed talus attributed to *Rudapithecus* (Kordos and Begun 2001; Begun 2002, 2009)—as well as *Oreopithecus* (Straus 1963; Szalay and Langdon 1986)—of controversial systematic affinities but currently interpreted as a likely stem hominoid (Pugh 2022; Urciuoli and Alba 2023; Alba, Urciuoli, et al. 2024).

To inform the evolution of ape locomotion, here we describe an unpublished talus (IPS85037) from the latest Middle Miocene of Abocador de Can Mata local stratigraphic sequence, previously attributed (without being described or figured) by Alba et al. (2017: table 2; 2022: SOM Table S6) to Dryopithecinae indet. The subfamily Dryopithecinae sensu Alba (2012) is an extinct group of Middle to Late Miocene great apes from Europe that is sometimes distinguished at the tribe rank (i.e., Dryopithecini) by some other authors (e.g., Begun 2009). Although they are generally considered extinct great apes (i.e., Hominidae; Alba 2012; Begun 2015; Urciuoli et al. 2021; Urciuoli and Alba 2023), as supported by cladistic analyses (Alba et al. 2015; Pugh 2022), it is still uncertain whether they constitute a clade or a paraphyletic assemblage (Alba 2012; Almécija et al. 2021). A consensus has yet to be reached as to whether dryopithecines are stem hominids (Andrews 1992; Casanovas-Vilar et al. 2011; Alba 2012; Alba et al. 2015) or crown hominids more closely related to either pongines (Moyà-Solà and Köhler 1993, 1995, 1996; Agustí et al. 1996) or hominines (Begun 2002, 2009, 2015, 2018; Begun et al. 2012). However, most recent cladistic analyses support the view that dryopithecines are stem hominids, with Late Miocene hispanopithecins (*Hispanopithecus* and *Rudapithecus*) occupying a more derived position toward crown hominids than the Middle Miocene dryopithecines (Pugh 2022). The dryopithecine talus described here was found isolated in a locality that has yielded no further primate remains (Alba et al. 2017). The size of the specimen discounts an attribution to the small-bodied catarrhines that have been recovered from ACM (Alba, Moyà-Solà, et al. 2010; Alba et al. 2015; Alba, Moyà-Solà, et al. 2012; Bouchet et al. 2024), but does not enable a conclusive assignment to any of the large-bodied dryopithecines recorded from slightly older sediments from the ACM sequence (Moyà-Solà et al. 2004; Moyà-Solà, Köhler, et al. 2009; Moyà-Solà, Alba, et al. 2009; Alba 2012; Alba and Moyà-Solà 2012; Alba et al. 2013, 2020; Alba, Bouchet, et al. 2024), namely *Pierolapithecus catalaunicus*, *Anoiapithecus brevirostris*, or *Dryopithecus fontani*.

Based on comparisons with extant anthropoid primates by means of three-dimensional geometric morphometric (3DGM) techniques, we evaluate the closest morphological affinities of the ACM dryopithecine talus and make locomotor inferences based on the covariation between talar shape and locomotor behavior, as well as additional morphofunctional considerations. During the last decade, 3DGM has been increasingly applied to the study of catarrhine talar morphology (Turley and Frost 2013), with emphasis on extant hominoids (Parr et al. 2011; Parr et al. 2014; Knigge et al. 2015; Friesen et al. 2024) and extinct hominins (Rosas et al. 2017; Sorrentino et al. 2020). However, to our knowledge, this is the first study where a Miocene ape talus is analyzed by means of 3DGM. All dryopithecines for which postcranial elements are available show a mosaic of plesiomorphic and apomorphic features that do not match the body plan found in any living ape—reflecting combinations of positional behaviors that have no modern analog (e.g., Alba 2012; Ward 2015; Almécija et al. 2021). Consequently, we predict that IPS85037 will not closely resemble the talar morphology of

any extant ape lineage. Instead, we expect that it will exhibit a mosaic morphology combining plesiomorphic ("monkey-like") and apomorphic (modern "hominoid-like") features. In addition, Middle Miocene dryopithecins are considered to be postcranially less derived than Late Miocene hispanopithecins, including *Danuvius* (Alba 2012; Almécija et al. 2021; Urciuoli and Alba 2023)—presumably lacking the suspensory specializations of the latter (Moyà-Solà et al. 2004; Moyà-Solà et al. 2005; Almécija et al. 2007; Almécija et al. 2009; Alba, Almécija, et al. 2010; Böhme et al. 2019; Pina et al. 2019; but see Begun and Ward 2005; Deane and Begun 2008, 2010). Thus, we also predict that IPS85037 will lack adaptations for suspensory locomotion, contrary to later hispanopithecins. Therefore, despite not being attributable to genus rank, the ACM dryopithecine talus not only provides new insight into the locomotor adaptations of dryopithecines but also contributes to a better understanding of talar morphology evolution and its locomotor implications in crown hominoids.

1.2 | Age and Geological Background

The ACM local stratigraphic sequence is located at els Hostalets de Pierola (Catalonia, Spain), in the Penedès sector of the Vallès-Penedès Basin (NE Iberian Peninsula). This basin is a Neogene half-graben limited by the Pre-Littoral and Littoral Catalan Coastal Ranges, close to Barcelona, that has yielded a rich fossil vertebrate record from the Early to the Late Miocene (Casanovas-Vilar, Madern, et al. 2016). The sedimentary deposits of the basin are broadly structured in two complexes of continental units, with intercalated marine and transitional units (Casanovas-Vilar, Madern, et al. 2016). The ACM stratigraphic sequence belongs to the upper continental complexes, which are Middle to Late Miocene in age (Alba et al. 2006, 2017; Moyà-Solà, Alba, et al. 2009; Casanovas-Vilar, Garcés, et al. 2016; Casanovas-Vilar, Madern, et al. 2016; Casanovas-Vilar et al. 2022). The sediments from ACM predominantly consist of mudstones, which were deposited in the distal-to-marginal, inter-fan zones of the coalescing alluvial fan systems of Olesa and els Hostalets de Pierola (Moyà-Solà, Köhler, et al. 2009; Casanovas-Vilar, Garcés, et al. 2016; Alba et al. 2017).

Based on litho-, bio-, and magnetostratigraphic correlation, the ACM sequence spans from 12.6 to 11.1 Ma (Middle to Late Miocene) and covers the Mammal Neogene (MN) zones MN6 (late portion), MN7+8, and MN9 (earliest portion), being correlated to the late Aragonian and earliest Vallesian (Casanovas-Vilar, Garcés, et al. 2016; Alba et al. 2017, 2022). The primate fossil talus described here was found isolated in the framework of paleontological surveillance performed during the construction of Sector B of Cell 8 of the Can Mata landfill in 2014. Its exact stratigraphic position (locality ACM/C8-B*) relative to the ACM composite sequence (Alba et al. 2017, 2022) was recorded, enabling a correlation with the base of normal polarity subchron C5r.2n, with an interpolated age of 11.65 Ma (Alba et al. 2022) that coincides with the Middle/Late Miocene (Serravallian/Tortonian) boundary (Raffi et al. 2020). Isotopic and mesowear data from the ACM fauna suggest that the time span comprised between 11.7 and 11.6 Ma at ACM was characterized by greater habitat heterogeneity than previous periods (DeMiguel et al. 2021), which might explain the coexistence

between large-bodied dryopithecines and the small-bodied crouzeliid *Pliobates* around this time (Alba et al. 2017; DeMiguel et al. 2021).

2 | Materials and Methods

2.1 | Studied Material and Comparative Sample

IPS85037 (Figure 1A–E) is housed at the Institut Català de Paleontologia Miquel Crusafont (ICP) in Sabadell, Spain. The fossil was compared with a broad sample of extant anthropoids using 3DGM techniques. The extant comparative sample comprises 68 tali from 22 primate species across 14 genera, providing good phylogenetic coverage (Table 1; see Figure 2 for a representation of the main groups and Table S1 for further details). A talus of the Early Miocene hominoid *Ekembo heseloni* (KMN-RU 2036) was also included in the comparative sample (Walker and Pickford 1983) to gain insight into the stem hominoid condition. Additionally, the morphological affinities between IPS85037 and other relevant tali from Miocene apes and extinct catarrhines are assessed to understand better the evolution of hominoid talar morphology and its locomotor implications.

2.2 | Surface Scanning

3D virtual models of the specimens from the comparative sample were derived from surface scans obtained using a Geomagic Capture scanner (3D Systems, Rock Hill, USA) and subsequently cleaned using Geomagic Wrap 2019 (3D Systems, Rock Hill, USA). In turn, IPS85037 was scanned using a NextEngineTM 3D scanner HD (NextEngine Inc., Santa Monica, USA) using high definition (HD) settings following the protocol detailed by Hammond et al. (2016). The scanner's range was adjusted to Macro settings and the highest possible resolution (160 points per square inch). The three final scans obtained—one 360° scan and two bracket scans (top and bottom)—were fused in Scan Studio PRO v. 1.7.3 (NextEngine Inc., Santa Monica, USA) to obtain the final surface mesh, which underwent postprocessing following standard protocols (Tocheri et al. 2011; Hammond et al. 2016) using Geomagic Studio 12 (3D Systems, Rock Hill, USA). Since the talus virtual models included in the comparative sample were from the left side (or had been mirrored to appear as such), the 3D model of IPS85037 was mirrored to perform the analyses. The virtual model from the described specimen is available from MorphoSource (File S1). Similarly, the talus belonging to *E. heseloni* (KMN RU 2036) was scanned from the original specimen using the same procedure as for IPS85037.

2.3 | Geometric Morphometrics

Landmark protocol To perform the 3DGM analyses, 36 landmarks were placed following a protocol devised to capture the overall talar shape (Figure 3; Table 2). All landmarks are type II/III except for landmark 32 (type I). The 3D models were landmarked using Landmark Editor v. 3.0.0.6 (Wiley et al. 2005). All analyses were performed in the statistical software R v. 4.4.0 (R Core Team 2024), using the visual interface RStudio desktop v. 2023.3.0.386 (RStudio Inc., Boston, USA). In addition,
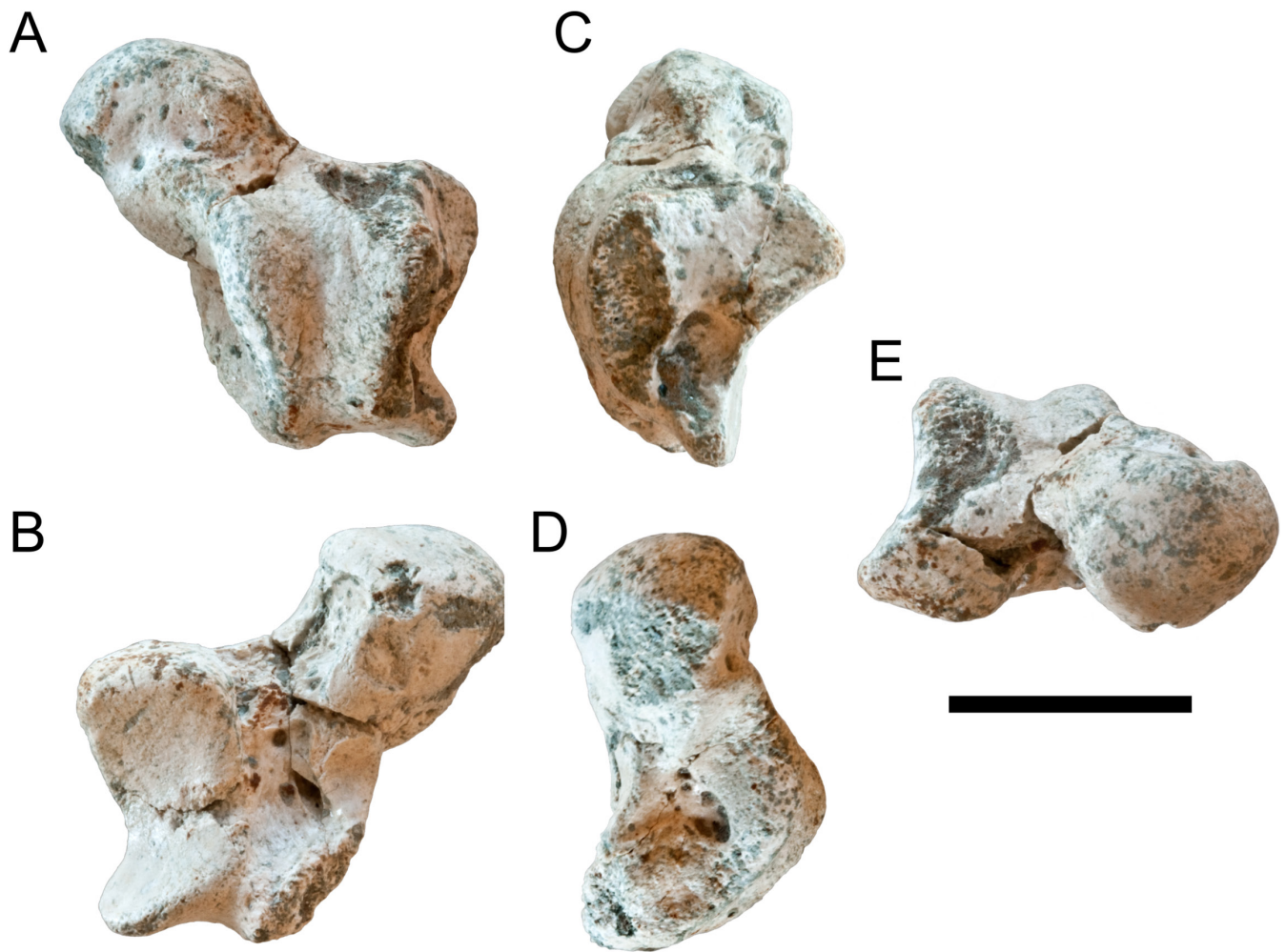
FIGURE 1 | IPS85037, right talus of Dryopithecini indet. from ACM/C8-B*, in dorsal (A), plantar (B), lateral (C), medial (D), and distal (E) views. Scale bar equals 2 cm.

a table with a list of 11 talar measurements using linear metrics (following Youlatos 1999) is provided for comparative purposes (Table 3). A generalized Procrustes analysis (GPA) was performed to obtain the Procrustes-aligned coordinates using "gpagen" function of "geomorph" package v. 4.0.7 (Adams and Otárola-Castillo 2013).

To confirm the repeatability of the landmark coordinate digitization used for geometric morphometric analyses (Shearer et al. 2017), intra- and inter-observer repeatability tests were performed by placing the same landmarks by four different researchers (Figure S1A) and four times by the same researcher (Figure S1B), respectively. Procrustes distances (Tables S2 and S3) and per-landmark variance (Figure S2; Table S4) were calculated. No significant differences were found between the intra- and inter-observer conditions ($t = 1.4035$, $p = 0.1651$), indicating that the landmark configuration is repeatable by different researchers.

Principal components analysis A between-group principal components analysis (bgPCA; Culhane et al. 2002) was performed on the Procrustes-aligned coordinates using the "groupPCA" function of "Morpho" package v. 2.12 (Schlager 2017). Four groups were defined a priori: platyrrhines, cercopithecoids,

hylobatids, and hominids. Unlike a standard PCA, a bgPCA maximizes variance along the axes based on the centroids (averages) of the groups defined a priori, with the scores of individual specimens being subsequently plotted post hoc onto the morphospace, thereby enhancing group distinction. The data from the fossil 3D models (IPS85037 and KMN-RU 2036) were projected a posteriori on each analysis. Bivariate plots among between-group principal components (bgPCs) were plotted using the "ggplot2" package v. 3.5.1 (Wickham 2016). For visualization purposes, a thin-plate spline deformation of the 3D model of a reference talus was carried out using the functions "shape.predictor" and "tps3d" of the "geomorph" and "Morpho" packages, respectively, and "shade3d" of the "rgl" package 1.1.3 (Adler and Murdoch 2020). The "mshape" and "findMeanSpec" functions of the package "geomorph" were used to find the closest specimen to the sample mean to use as the reference. The specimen selected was a talus of *Pan paniscus* (RMCA 27698).

To assess the presence of allometric effects, the three resulting bgPCs were regressed using the ordinary least-squares method (OLS) against natural log-transformed (ln) centroid size of the talus for each specimen using the "procD.lm" function in "geomorph" and plotted using the package "ggplot2." To address the concerns about potentially spurious grouping

TABLE 1 | Summary of the comparative sample of extant anthropoid tali used in this study.

| Main group	Species	Males	Females	Total
Platyrrhini	*Alouatta palliata*	1	1	2
Platyrrhini	*Alouatta seniculus*	1	1	2
Platyrrhini	*Ateles fusciceps*	2	2	4
Platyrrhini	*Cebus apella*	3	1	4
Cercopithecidae	*Colobus guereza*	2	2	4
Cercopithecidae	*Macaca artoides*	0	1	1
Cercopithecidae	*Macaca fascicularis*	1	0	1
Cercopithecidae	*Macaca mulatta*	1	1	2
Cercopithecidae	*Nasalis larvatus*	1	1	2
Cercopithecidae	*Papio anubis*	1	1	2
Cercopithecidae	*Papio hamadryas*	0	1	1
Hylobatidae	*Hylobates agilis*	0	1	1
Hylobatidae	*Hylobates klossii*	1	0	1
Hylobatidae	*Nomascus concolor*	1	0	1
Hylobatidae	*Symphalangus syndactylus*	1	2	3
Hominidae	*Gorilla beringei*	5	2	7
Hominidae	*Gorilla gorilla*	3	3	6
Hominidae	*Homo sapiens*	2	2	4
Hominidae	*Pan paniscus*	2	2	4
Hominidae	*Pan troglodytes*	5	3	8
Hominidae	*Pongo abelii*	1	1	2
Hominidae	*Pongo pygmaeus*	3	3	6
Total		37	31	68

when bgPCA is applied to highly multidimensional datasets (Bookstein 2019; Cardini et al. 2019)—such as those coming from 3DGM analyses—we designed the sample to include groups with a large number of individuals (Rohlf 2021). We also followed Cardini and Polly's (2020) recommendation to perform a cross-validated bgPCA on the raw data using the "groupPCA" function of the package "Morpho." With the same aim in mind, we also computed group mean differences for the raw shape data, regular bgPCA scores, and cross-validated bgPCA scores using the "lm.rrpp" function of the R package "RRPP" v. 2.0.0 (Collyer and Adams 2018). In addition, a standard PCA was performed to evaluate the differences between the bgPCA and a standard PCA using "prcompfast" function of "Morpho." In this second case, 3D data of IPS85037 and KMN-RU 2036 were projected a posteriori onto the morphospace defined by extant taxa.

Finally, we computed the typicality probabilities of group membership for the fossil specimens using the "typprobClass" function of the "Morpho" package. Unlike posterior probabilities, which are customarily calculated in discriminant analyses and assume that classified individuals belong to one of the a priori defined groups, typicality probabilities evaluate the similarity of a specimen to each group separately. Although the classification of each specimen is similarly based on the highest probability, the typicality probabilities also represent the *p* value to test the null hypothesis of group membership (separately for each group). Thus, even if the highest typicality probability denotes the highest morphometric affinities, it might still indicate that the specimen does not fit within the variation of the group if $p < 0.05$.

2.4 | Body Mass Estimation

Talus size, as captured using either linear measurements (e.g., Tsubamoto et al. 2016), articular areas (e.g., Yapuncich et al. 2015), or centroid size in 3DGM analyses (e.g., Parr et al. 2014), has been established as a suitable proxy of body mass (BM). We followed the latter approach to estimate BM for the described dryopithecine talus. As the comparative sample does not include individuals of known BM, mean data (Table S5) for both males and females of each species were taken from the literature (Smith and Jungers 1997). In the
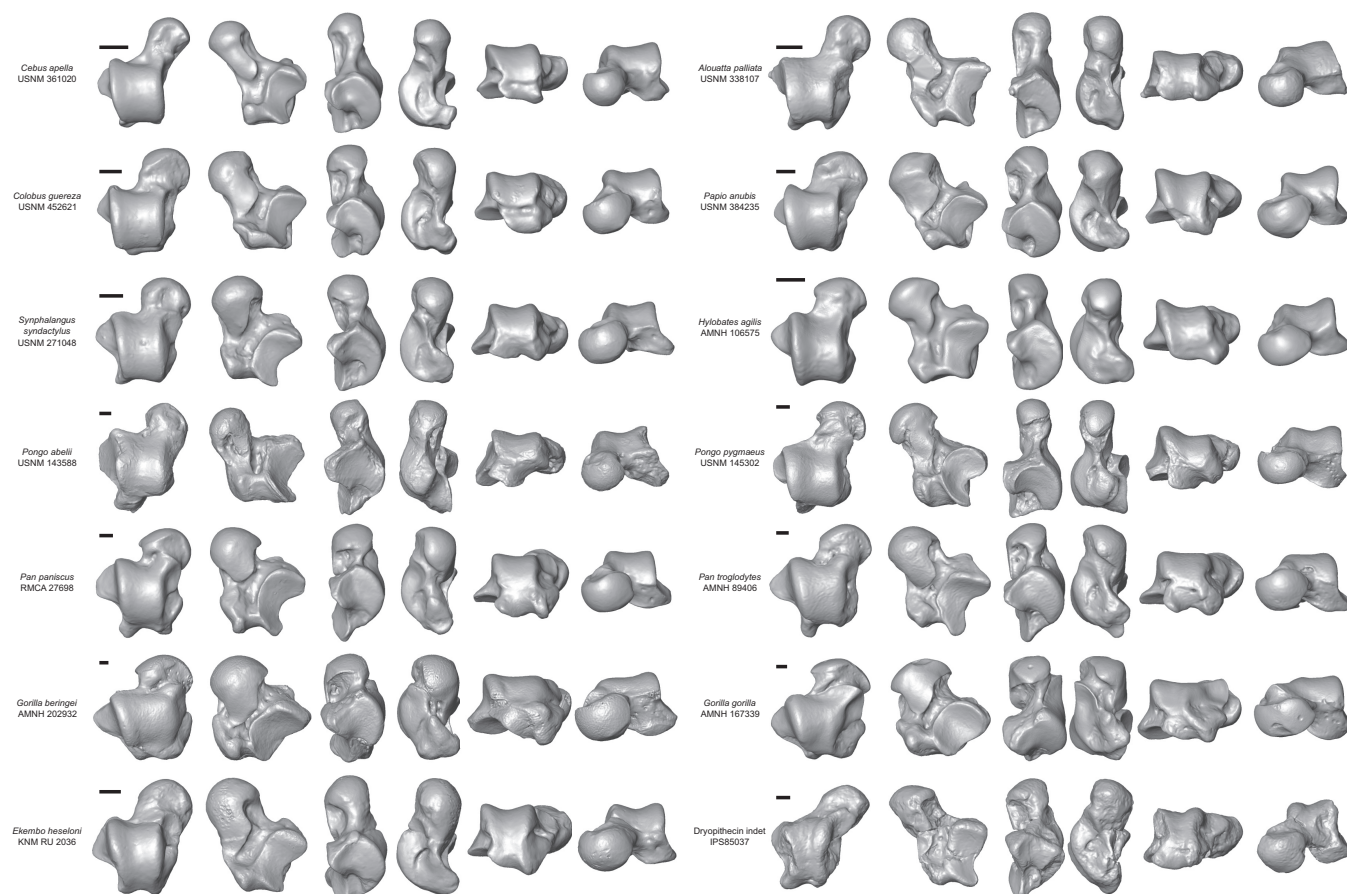
FIGURE 2 | Render images of the talus of Dryopithecini indet. from ACM/C8-B* (IPS85037) as compared to that of *Ekembo heseloni* (KMN RU 2036) and a selected sample of tali from extant anthropoids included in the comparative sample; from left to right, in dorsal, plantar, lateral, medial, and distal views. Scale bars equal 5 mm.

case of polytypic species, the average of subspecies BM means was computed for each sex. To estimate BM, allometric regressions of ln BM vs. ln centroid size were performed using an OLS regression with the "lm" function of the "stats" package. Body mass estimates for IPS85037 and KMN-RU 2036 were derived from the best-fit regression line by further applying the quasi-maximum likelihood estimator (QMLE) to account for the logarithmic transformation bias (Smith 1993). The latter was computed as $QMLE = \exp(SEE^2/2)$, where SEE is the standard error of estimate of the regression. 50% and 95% confidence intervals (CIs) were computed for each BM estimate of the fossil specimen.

2.5 | Partial Least-Squares Regression

Previous studies (e.g., Püschel et al. 2018, 2020; Llera Martín et al. 2022) have shown that it is possible to distinguish between main locomotor modes and substrate preferences using tarsal shape, as well as to infer the locomotor behavior of fossil primates on its basis. These studies discretized locomotor categories or substrate preferences into a limited number of categories to enable the application of different classification algorithms. Although certainly valuable, these approaches have limitations that arise from the fact that any classification scheme is a simplification of the actual locomotor repertoire displayed by any primate species, which includes a variety of locomotor behaviors.

Other studies have overcome such limitations using two-block partial least-squares analysis (2B-PLS; Rohlf and Corti 2000), which enables the assessment of major patterns of covariation between a shape data matrix (e.g., talar shape) and a locomotor behavior data matrix (e.g., Almécija et al. 2015; Fabre et al. 2017; Fabre et al. 2018; Fabre et al. 2019; Püschel et al. 2017). These studies have shown that it is possible to find strong covariation patterns between behavioral data (e.g., locomotion) and the shape of certain skeletal elements, which may be used to make paleobiological inferences. However, the aforementioned works only focused on extant species and did not try to infer the locomotor behavior of extinct taxa. In addition, the standard version of 2B-PLS in the morphometric literature is a symmetric analysis that, in its classic formulation, does not allow predictions (Zelditch et al. 2012). However, there is a type of partial least-squares analysis more comparable to regression, known as partial least-squares regression (PLSR), that allows the generation of predictive models (Wold et al. 2001). This method has been previously applied in geometric morphometrics to predict one block of shape variables from another one (e.g., Schlager 2013; Archer et al. 2018; Bastir et al. 2019; Torres-Tamayo et al. 2020), and recently has been used to estimate the locomotor behavior of early primate species, yielding a good predictive performance (Monclús-Gonzalo et al. 2023). Therefore, we applied a PLSR approach to infer the locomotor behavior of the two Miocene apes included in the studied and comparative samples based on their talar shape.
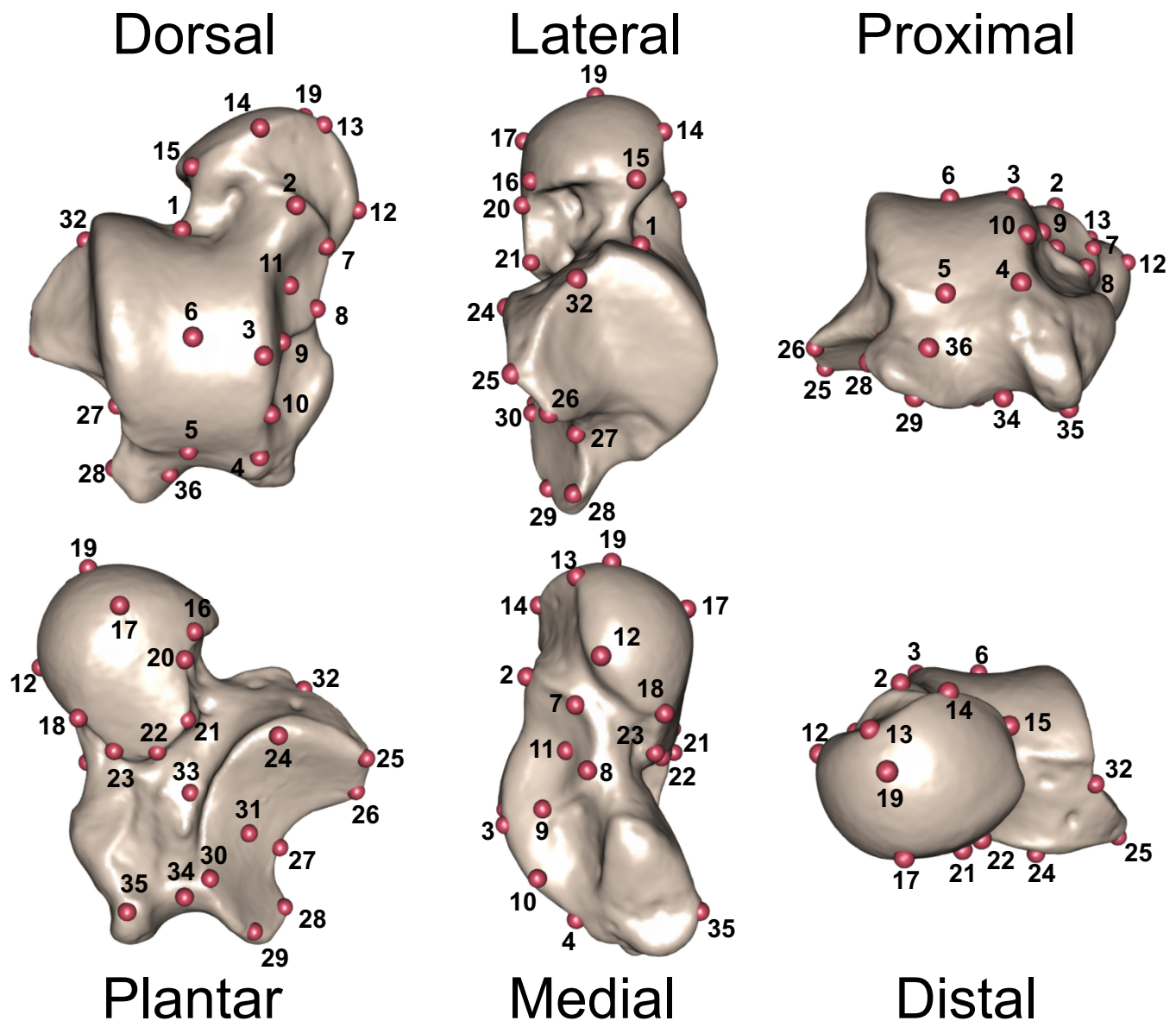
FIGURE 3 | Landmark configuration utilized in this study (see Table 2 for landmark definitions). The specimen used as reference corresponds to the talus of *Pan paniscus* (RMCA 27698).

The two blocks of data consisted of (1) talar shape (Procrustes-aligned coordinates) averaged by species and (2) locomotor mode percentages (LMPs)—that is, the percentage time a species spends performing a certain locomotor behavior—for the 21 extant species included in the extant comparative sample. Locomotor data were taken from the literature (see references in Table S6). Five locomotor modes were distinguished: (1) quadrupedal walking, bounding, and running; (2) clambering and vertical climbing; (3) leaping, dropping, and hopping; (4) bridging, brachiation, and suspensory locomotion; and (5) bipedal walking. Because the locomotor data came from different sources, and not all behaviors reported in the original studies were considered, we rounded the LMPs to percentages for those species that included small amounts of locomotor modes not considered in this study, ensuring that they add up to 100%. In addition, to ensure that our locomotor predictions were between 0% and 100%, we first converted the percentages to proportions by dividing them by 100 and then we applied a logit transformation, which can be defined as ln [$P/(1-P)$], where P is a proportion

(Cramer 2003). This transformation was done prior to carrying out the PLSR to avoid nonsensical results (e.g., LMPs higher than 100% or lower than 0%). Given that ln (0) is undefined, we added 1% to any LMP equal to 0 and then we rounded up the LMPs again to ensure that they added up to 100% before carrying out the logit transformation.

The PLSR is based on the same basic machinery as the standard 2B-PLS, which means that it finds the principal components of covariation between the blocks of variables by means of decomposing the covariance matrix of the two blocks into two sets of eigenvectors (one for each set of variables) and eigenvalues, using a singular value decomposition to generate a matrix of singular values (the square roots of the eigenvalues), a matrix of eigenvectors for the first set of variables and the transpose of the matrix of eigenvectors for the second set of variables (Rohlf and Corti 2000). We carried out this step by using the "two.b.pls" function of the "geomorph" package, and we ran 9999 iterations for significance testing. The PLSR

TABLE 2 | Definition of the 36 landmarks used in this study.

Landmark	Name/Structure	Description
1	Trochlear surface	Point of maximum concavity on distal margin
2		Most disto-tibial point
3		Most dorsally convex point along tibial border
4		Most proximo-tibial point
5		Point of most inflection along the proximal margin
6		Most proximal point along the trochlear groove between 1 and 5
7	Tibial malleolar surface	Most disto-tibal point
8		Most proximo-plantar point
9		Point of most inflection along margin between 8 & 10
10		Most proximal point
11		Most concave point on distal portion of surface
12	Talar head	Most dorso-tibial point
13		Most distal point along dorsal margin
14		Most dorsally convex point along margin between 13 and 15
15		Most fibular point
16		Point of most distal inflection along ridge between 15 and 20
17		Most distal point along margin with anterior subtalar facet
18		Most planto-tibial point
19		Most distally extending point on surface
20	Anterior subtalar surface	Point of most inflection on disto-fibular margin
21		Most fibularly extending point
22		Most convex point along margin between 21 and 23
23		Most proximo-tibial point
24	Posterior subtalar surface	Most disto-tibial point
25		Most disto-fibular point
26		Most convex point along margin between 25 and 27
27		Point of most inflection on proximo-fibular margin
28		Point of greatest convexity along margin between 27 and 29
29		Most proximo-fibular point
30		Most proximo-tibial point
31		Most plantarly concave point around center of surface
32	Fibular malleolar surface	Distal junction of the lateral trochlear rim and the fibular malleolar surface
33	Sulcus tali	Deepest point at the level of maximum tibial concavity
34		Deepest point around tibio-fibular axis
35		Tip of tibial margin
36	Posterior process	Midpoint root on proximo-dorsal side

works by regressing the first block of variables on the vector obtained from the scores for the second block of variables (i.e., the LMPs were regressed on the talar shape values that were projected onto the obtained singular vectors). This step was done using the "procD.lm" function of the same package (9999 iterations were used). To obtain LMP predictions, the talar

TABLE 3 | Talar linear measurements for IPS85037 (following Youlatos 1999).

	AS1	AS2	AS3	AS4	AS5	AS6	AS7	AS8	AS9	AS10	AS11
IPS85037	8.7	8.6	14.5	36.5	4.8	20.7	15.5	17.1	14.3	(17.8)	(13.2)

Abbreviations: AS1 = length of tibial malleolar surface on the dorsomedial plane; AS2 = length of the neck on the dorsolateral plane; AS3 = maximum length of the neck and head; AS4 = maximum length of the talus; AS5 = height of the posterior subtalar facet; AS6 = length of the posterior subtalar facet; AS7 = length of the head; AS8 = height of the head, perpendicular to the former measurement; AS9 = maximum length of the neck on the dorsal plane; AS10 = distal length of the trochlea; AS11 = proximal length of the trochlea.

shape values were projected onto the obtained singular vectors and then multiplied by a matrix consisting of the linear model coefficients. This process was done with the talar shape (Procrustes-aligned coordinates) averaged for extinct species to derive locomotor inferences (i.e., estimated percentages for the various locomotor modes). Given that, prior to the PLSR, the LMPs were subjected to a logit transformation, the obtained predictions were transformed back into percentages by applying an inverse logit transformation, defined as $\exp(X)/[1 + \exp(X)]$, where X corresponds to a logit transformed value. The obtained predictions were then rounded up again to ensure that they added to 100%. To assess the PLSR predictive performance, we performed a "leave-one-out cross-validation" (LOOCV), which means that separate analyses were carried out for each one of the predictions, excluding the particular individual for which the prediction was being calculated (Kuhn and Johnson 2013). Using these cross-validated results, we computed the mean absolute error (MAE; i.e., the arithmetic average of the absolute errors) to assess our prediction results using the extant sample (Willmott and Matsuura 2005).

Additionally, the talus specimen closest to the multivariate mean of the talar shape dataset (*Pan paniscus*, RMCA 27698) was warped to represent the covariation between shape and LMPs along the first singular vectors (following the same procedure as that explained above to visualize the shapes associated to the negative and positive extremes of each axis of the bgPCA). A principal component analysis (PCA) was carried out with the LMPs using the "prcomp" function of the R package "stats." The PCA scores and the loadings of each locomotor variable were assembled in the same scatterplot (as a biplot). The estimated locomotor repertoires of IPS85037 and KMN RU 2036 were projected onto the PCA to visualize their placement within the "ecospace" defined by extant species' locomotor behavior. The direction and length of each vector indicate the region of the scatterplot in which the locomotor variable is more represented. As a result, those specimens projected the furthest in the direction of a given vector are those whose locomotor repertoire possesses the highest percentage in the direction of the corresponding locomotor variable.

3 | Results

3.1 | Description

The right talus IPS85037 (Figure 1A–E) is well preserved except for minor damage on the lateral edge of the trochlea, the medial tubercle, the posterior calcaneal facet, and the medial edge of the talar head, as well as a crack at the level of the neck. The talar body is dorsoplantarly taller than mediolaterally wide. The trochlea is wedge-shaped (broader anteriorly than posteriorly), displays a moderately deep central groove, and has a slightly dorsoplantarly higher lateral trochlear rim compared to the medial one. The groove for the flexor hallucis longus tendon is placed in a mid-trochlear position, flanked by a well-developed posterior lateral tubercle and a similarly developed (but somewhat damaged) posterior medial tubercle. The articular facet with the fibula is relatively dorsoplantarly tall and moderately expanded laterally. The medial tibial facet is moderately steep and does not reach the plantar side of the bone. The neck is relatively long and slender, medially angled, has a subsquare cross-section almost as wide as high, and displays a strong medial orientation. The posterior calcaneal facet is relatively shallow, subsquare (except for its proximal edge, which tapers toward the medial tubercle), slightly concave, and obliquely oriented. The sulcus tali is relatively broad and shallow. The anterior calcaneal facet is continuous and mediolaterally narrow, extending up to the anterior end of the sulcus tali. The talar head, relatively small and ovoid, bears a markedly convex articular surface that extends more laterally than medially and shows a slight medial torsion.

3.2 | Comparison With Stem Catarrhine and Other Miocene Ape Tali

The trochlear morphology of IPS85037, like that of stem catarrhines and other Miocene apes, exhibits an anteriorly broad articular facet and a relatively deep trochlear depth comparable to the dendropithecid *Simiolus enjiessi* (Leakey and Leakey 1987; Rose et al. 1992), the pliopithecoid *Pliopithecus antiquus* (see Senut 2012), and most Miocene hominoids (*E. heseloni*, *Ekembo nyanzae*, *Equatorius africanus*, *Nacholapithecus kerioi*, and *Sivapithecus sivalensis*; MacInnes 1943; Le Gros Clark and Leakey 1951; Pilbeam et al. 1980; Harrison 1982; Walker and Pickford 1983; Leakey and Leakey 1987; Rose et al. 1992, 1996; McCrossin 1994; Madar 1996; Ishida et al. 2004; Nakatsukasa et al. 2012). It differs from the dendropithecid *Dendropithecus maccinesi* (Le Gros Clark and Thomas 1951) and the nyanzapithecid *Rangwapithecus gordoni* (DeSilva 2008) in displaying a deeper trochlear groove. The lateral trochlear rim of IPS85037 is only slightly higher than the medial rim, as in extant hominoids (particularly orangutans and hylobatids; Turley and Frost 2013), dendropithecids (*D. maccinesi* and *S. enjiessi*; Le Gros Clark and Thomas 1951; Leakey and Leakey 1987; Rose et al. 1992), *Oreopithecus* (Szalay and Langdon 1986), and the stem pongine *Si. sivalensis* (Pilbeam et al. 1980; Madar 1996). Conversely, the lateral trochlear rim of IPS85037 is less prominent than that of extant cercopithecoids (Strasser 1988), pliopithecoids (*P. antiquus* and *Anapithecus hernyaki*; Begun 1987; Senut 2012), and several stem hominoids (*Turkanapithecus kalakolensis*, *E. heseloni*, *E. nyanzae*, *Eq. africanus*, and *N. kerioi*; Harrison 1982; Walker and Pickford 1983; Leakey and Leakey 1987; Ward

et al. 1993; McCrossin 1994; Ishida et al. 2004; Nakatsukasa et al. 2012).

Posteriorly, IPS85037 displays a deep and well-defined groove for the tendon of the m. flexor hallucis longus, and a rather well-developed posterior lateral tubercle. This condition is also met by the stem hominoid *Proconsul major* and *Orepithecus* (Harrison 1982; Szalay and Langdon 1986; DeSilva 2008). IPS85037 further resembles the afropithecid *N. kerioi* in the well-developed lateral posterior tubercle (Ishida et al. 2004; Nakatsukasa et al. 2012). Conversely, the condition of IPS85037 is markedly distinct from the shallow groove displayed by pliopithecoids (Begun 1987; Senut 2012) and the afropithecid *Eq. africanus* (McCrossin 1994). Moreover, IPS85037 resembles extant hominoids in the less concave facet for the medial tibial malleolus and the lack of a dorsal ridge on the talar neck (Conroy and Rose 1983). In the latter feature, IPS85037 is similar to *R. gordoni*, *Pr. major*, and *O. bambolii* (Harrison 1982; Szalay and Langdon 1986; DeSilva 2008) but different from the deeply cupped facet and the pronounced dorsal ridge exhibited by pliopithecoids (*P. antiquus* and *Epipliopithecus vindobonensis*; Zapfe 1958; Senut 2012), dendropithecids (*Micropithecus songhorensis* and *S. enjiessi*; Le Gros Clark and Thomas 1951; Leakey and Leakey 1987; Rose et al. 1992) and several stem hominoids (*E. heseloni*, *E. nyanzae*, *Eq. africanus*, and *N kerioi*; MacInnes 1943; Le Gros Clark and Leakey 1951; Harrison 1982; Walker and Pickford 1983; Leakey and Leakey 1987; Rose et al. 1992, 1996; McCrossin 1994; Ishida et al. 2004; Nakatsukasa et al. 2012), which resemble instead the extant cercopithecoids (Le Gros Clark and Leakey 1951; Harrison 1982).

IPS85037 resembles most stem catarrhines and Miocene apes in the gracile and moderately elongate neck (Harrison 1982), with the exception of *O. bambolii*, which resembles extant hominoids (excluding orangutans) in the extremely abbreviated neck (Szalay and Langdon 1986). In contrast, IPS85037 resembles *O. bambolii* and differs from other Miocene apes and stem catarrhines in the medially angled neck, albeit less markedly so than in *O. bambolii* (Szalay and Langdon 1986). IPS85037 resembles the pliopithecoid *P. antiquus* (Senut 2012), as well as the stem hominoids *T. kalakolensis* (Leakey and Leakey 1987) and *Pr. major* (Harrison 1982; DeSilva 2008) in the small and spherical head. In contrast, IPS85037 differs in this regard from dendropithecids (*D. maccinesi* and *S. enjiessi*; Le Gros Clark and Thomas 1951; Leakey and Leakey 1987; Rose et al. 1992) and several Miocene apes (*E. heseloni*, *E. nyanzae*, *Eq. africanus*, *N. kerioi*, and *O. bambolii*; MacInnes 1943; Le Gros Clark and Leakey 1951; Harrison 1982; Walker and Pickford 1983; Szalay and Langdon 1986; Rose et al. 1996; Ward et al. 1993; McCrossin 1994; Ishida et al. 2004; Nakatsukasa et al. 2012), which exhibit mediolaterally broad and large heads like those of extant cercopithecoids and African apes.
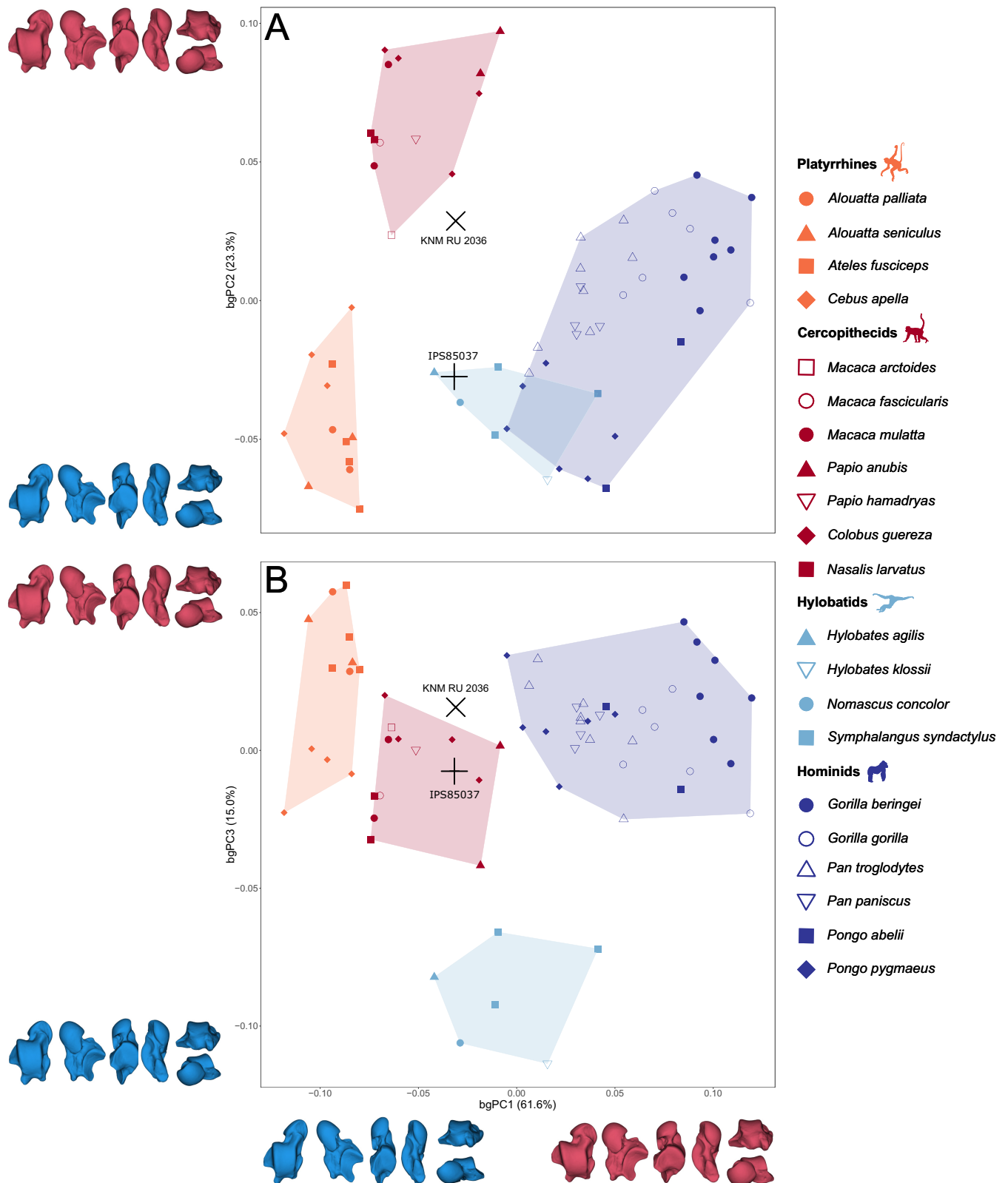
IPS85037 has a relatively flat and proximodistally elongated posterior calcaneal facet, comparable to that of orangutans (Langdon 1986). In this regard, IPS85037 differs from stem catarrhines and Miocene apes except for *O. bambolii* (Harrison 1982; Conroy and Rose 1983; Langdon 1986), which, like IPS85037, possesses a shallow and elongated facet (Szalay and Langdon 1986). Moreover, IPS85037 displays a small divergence between the posterior calcaneal facet and the long axis of the trochlea, matching extant hominoids, the pliopithecoid *An. hernyaki* (Begun 1987), *N. kerioi* (Ishida et al. 2004; Nakatsukasa et al. 2012), and *Si. sivalensis* (Pilbeam et al. 1980; Madar 1996). The sulcus tali of IPS85037, separating the anterior calcaneal facet from the posterior, is intermediate between the condition of extant great apes (deep and narrow) and gibbons and non-hominoid anthropoids (shallow and broad; Harrison 1982). Finally, IPS85037 resembles stem catarrhines and most other Miocene apes in the anteromedially L-shaped anterior calcaneal facet (Harrison 1982), except for *O. bambolii*, which differs from IPS85037 and resembles extant hominoids in possessing a crescent-shaped facet (Szalay and Langdon 1986).

3.3 | Morphometric Comparisons

The bgPCA (Figure 4) correctly classifies 100% of cases in the four extant groups defined a priori (platyrrhines, cercopithecoids, hylobatids, and hominids), whereas the bgPCA with cross-validation (Figure S3A,B) correctly classifies 94% of cases (Tables S7 and S8). The similarities between standard PC scores (Figure S4A,B) and standard and cross-validated bgPC scores suggest that discrimination is not spurious. In addition, significant group differences in the raw shape data indicate the presence of group structure in our sample ($R^2 = 0.23$, $p < 0.001$). Even if the amount of variance increases considerably when group differences are computed for bgPC ($R^2 = 0.77$, $p < 0.001$) and cross-validated bgPC scores ($R^2 = 0.71$, $p < 0.001$), the overall similarities between the Z-scores computed for the raw data ($Z = 6.49$), bgPC scores ($Z = 13.79$), and cross-validated bgPC scores ($Z = 12.01$) allow us to reject the presence of spurious grouping in the analysis.

The bgPC1 (62% of total variance; Figure 4A,B) reflects differences in talar body shape (broader and stouter toward positive scores vs. slenderer toward negative scores), wedging of the trochlea (broader anteriorly than posteriorly toward positive scores vs. subparallel rims toward negative scores), the shape of the posterior calcaneal facet (slenderer and medially tapered toward negative scores and broader and more squared toward positive scores), the anterior calcaneal facet (proximodistally longer and mediolaterally narrow toward positive scores and broader and more proximodistally restricted toward negative scores), proximodistal elongation and robusticity of the talar neck (shorter and more robust toward positive scores and proximodistally longer and slenderer toward negative scores), and the relative size of the talar head (smaller and more spherical toward negative scores). This axis separates platyrrhines (negative end of the axis) from cercopithecoids (moderately negative scores) as well as hylobatids (moderately negative or positive scores) and hominids (mostly positive scores), with hylobatids partly overlapping with both cercopithecoids and hominids. A significant allometric relationship is found between bgPC1 and talus size, indicating a strong positive correlation that accounts for 78% of the variance (Figure S5A, Table 4). This result parallels the rough gradient of decreasing body size observed along bgPC1, although hylobatids exhibit comparably more positive scores (overlapping with the lower end of great apes) than expected given their body size, while monkeys (especially platyrrhines), in contrast, display lower bgPC1 values than that expected on this basis.

FIGURE 4 | Results of the between-group principal components analysis (bgPCA) as depicted by a bivariate plot of bgPC2 vs. bgPC1 (A) and bgPC3 vs. bgPC1 (B). The groups distinguished a priori are indicated by color-coded convex hulls, and each species is denoted by different symbols, as indicated in the legend. Fossil specimens (whose scores are projected a posteriori) are indicated by a cross (✕) sign (KMN RU 2036) and a plus (+) sign (IPS85037). The percentage of variance explained by each bgPC is reported within parentheses. Talar shapes associated with minimum (blue) and maximum (red) values of each bgPC axis are plotted below each scatterplot (dorsal, plantar, lateral, medial, proximal, and distal views are shown from left to right). Thin plate spline warps are based on a talus of *Pan paniscus* (RMCA 27698).

TABLE 4 | Ordinary least-squares regressions of between-group principal components (bgPCs) vs. log-transformed centroid size (ln CS).[a]

bgPC	Slope	Intercept	r^2	Z	p
bgPC1	0.141	−0.611	0.758	6.777	**< 0.001**
bgPC2	0.011	−0.046	0.010	0.195	0.439
bgPC3	0.026	−0.113	0.093	2.008	**0.016**

Note: Z = effect sizes (computed as standard deviates of Fischer's F).
[a]Significant results ($p < 0.05$) are indicated in bold.

The bgPC2 (23% of the variance; Figure 4A) is driven by the shape of the talar body (negative scores are associated with a shallower and more dorsoplantarly compressed trochlea and positive scores with a deeper and dorsoplantarly higher trochlea), the relative height of the lateral rim (more symmetrical rims toward negative scores and distinctly dorsoplantarly higher lateral rim, compared to the medial rim, associated with positive scores), the size of the posterior lateral tubercle and the development of the groove for the flexor hallucis longus tendon (smaller tubercle and less well-developed groove toward positive scores), the shape of the posterior calcaneal facet (mediolaterally broader facet more extended medially than laterally toward positive scores), and the anterior calcaneal facet (more concave toward negative scores). This axis separates the more arboreal and/or suspensory species (platyrrhines, hylobatids, and orangutans), which display negative scores, from the more cursorial cercopithecoids (positive scores). African apes display intermediate scores and overlap slightly with cercopithecoids and only minimally (especially in the case of chimpanzees) with other platyrrhines, hylobatids, and orangutans. Unlike bgPC1, bgPC2 is not significantly correlated with talar centroid size (Figure S5B; Table 4), indicating that shape changes along this axis are not affected by size-scaling effects. The bgPC2 seemingly reflects differences in locomotor behavior, with the most arboreal and suspensory hominoids (hylobatids and orangutans) overlapping with the suspensory platyrrhines (*Ateles* and, to a lesser extent, *Alouatta*). Non-suspensory platyrrhines (*Cebus*) also overlap with hylobatids and orangutans, but remarkably exhibit less negative scores than either *Ateles* or *Alouatta*. The bgPC2 shows a locomotor gradient, with terrestrial and semiterrestrial species displaying more positive scores than arboreal ones—except for committed arboreal cercopithecoids such as *Colobus* or *Nasalis*, which cluster with (semi)terrestrial cercopithecoids instead of other arboreal species.

The bgPC3 (15% of total variance; Figure 4B) reflects differences in the shape of the trochlea (increased wedging toward positive

scores), the size of the lateral posterior tubercle, and the depth of the groove for the flexor hallucis longus tendon (larger tubercle and deeper groove toward positive scores), and the shape of the anterior calcaneal facet (proximodistally more elongated toward positive values). This axis clearly discriminates hylobatids (very negative scores) from the rest of the comparative sample (which extensively overlaps from intermediate to moderately positive scores). The bgPC3 is significantly correlated with talus size (Figure S5C; Table 4). However, allometric effects can be excluded as the main driver of variation along this axis, as they only explain 8% of shape variance—as further illustrated by the overlap between great apes with the much smaller monkeys and the segregation of hylobatids from all monkeys irrespective of size.

Along bgPC1, both IPS85037 and KMN-RU 2036, characterized by a mediolaterally narrow and dorsoplantarly high astragalar body and a proximodistally elongated neck, overlap with hylobatids and cercopithecoids (Figure 4). Regarding bgPC2 (Figure 4A), IPS85037 closely approaches the variation of hylobatids and overlaps with that of the suspensory orangutans and atelids, as well as cebids. In contrast, KMN-RU 2036 displays a more positive score that approaches the cercopithecoid condition and overlaps with the knuckle-walking African apes. The different scores along bgPC2 can be explained by differences in talar shape between the two fossil specimens. IPS85037 shows some remarkable similarities with the tali of pongines and hylobatids, such as a slightly prominent lateral rim, a well-developed groove for the flexor hallucis longus tendon, and medial and lateral tubercles, a shallow and slightly angled (relative to the long axis of the bone) posterior calcaneal facet, a proximodistally elongated and medially angled neck, and a spherical and convex talar head. In contrast, KMN-RU 2036 more closely approaches the cercopithecoid condition in these regards. Finally, both IPS85037 and KMN-RU 2036 are distinguished from hylobatids along bgPC3 (Figure 4B), as both tali display a relatively wedged and dorsoplantarly deeper trochlea, as well as a more developed groove for the flexor hallucis longus tendon, similarly to the remaining taxa. The differences between the two fossil tali are further confirmed by the typicality probabilities (Table 5), with IPS85037 showing greatest affinities with platyrrhines but further matching the great ape variation, whereas KMN-RU 2036 is classified as a cercopithecoid despite not being incompatible either with the platyrrhine variation.

3.4 | Body Mass Estimation

The allometric equation derived to estimate body size is reported in Table 6. The BM estimate for IPS85037 is 38 kg (95%

TABLE 5 | Typicality probabilities[a] for individual fossil specimens based on a between-group principal component analysis on the Procrustes-aligned coordinates of each talar specimen carried out using four groups distinguished a priori among the extant comparative sample.

	Cercopithecidae	Hominidae	Hylobatidae	Platyrrhini
IPS85037	0.002	**0.041**	0.002	**0.104**
KNM RU 2036	**0.163**	0.004	< 0.001	**0.060**

[a]They indicate the probability of obtaining the score of each fossil specimen given membership in one of the a priori designed groups. Typicality probabilities above significance ($p \geq 0.05$) are bolded, while those below ($p < 0.05$) denote outliers to the distribution of each group.

TABLE 6 | Body mass (BM) estimates (in kg) based on centroid size (CS) using an ordinary least-squares allometric regression[a] of sex-species means (SOM Table S2).

	ln CS	BM estimate	CI (95%)	CI (50%)
IPS85037	4.476	38.008	34.695–41.637	36.863–39.189
KMN RU 2036	4.106	13.460	12.505–14.489	13.132–13.797

[a]ln BM = 2.808 × ln CS – 8.953 (r^2 = 0.963; p < 0.001; standard error of estimate = 0.213; quasi-maximum likelihood estimate = 1.023).

TABLE 7 | Results of the two-block partial least-squares (PLS) regression between talar shape and quantified locomotor data.[a]

Latent variable	Singular value	% covariance	r-PLS	*p*
PLS1	0.151	76.564	0.917	**< 0.001**
PLS2	0.067	15.066	0.868	**0.004**
PLS3	0.043	6.290	0.746	**0.008**
PLS4	0.022	1.577	0.749	0.206
PLS5	0.012	0.504	0.740	0.210

[a]Significant results (p < 0.05) are indicated in bold.

CI = 35–42 kg), thus being roughly the average size of a female orangutan (Smith and Jungers 1997). Conversely, the BM estimate for KMN RU 2036 is 13 kg (95% CI = 12–14 kg), comparable to male siamangs and slightly larger than most atelids, and similar to male macaques as well as female baboons (Smith and Jungers 1997).

3.5 | Partial Least-Squares Regression

The covariation between talar shape and locomotor behavior is significant and explains a considerable amount (92%) of covariance in the first two PLS axes (Table 7). The PLSR predictive performance is presented in Figure S6A–E and Tables S9 and S10.

The first axis (PLS1; Figure 5A; 77% of covariance) discriminates between most suspensory species (*Pongo*, hylobatids), in the most positive scores of the shape axis, and the most quadrupedal ones (African apes, cercopithecoids), located at the negative side of the axis. Platyrrhines, which engage in a more generalized locomotor behavior—including moderate amounts of arboreal quadrupedalism, climbing, and clambering, as well as some leaping (although some species, particularly atelids, also display tail-assisted suspensory behaviors)—are located in intermediate scores of the shape axis. Suspensory species are associated with a proximodistally longer trochlea, more symmetrical rims, a more laterally flaring fibular facet with a more gently inclined slope, a deeper groove for the flexor fibularis tendon and more developed posterior lateral tubercle, a shallower, narrower, and more

elongated posterior calcaneal facet, a shallower sulcus talus, and a smaller and more spherical talar head. Conversely, most quadrupedal species exhibit a mediolaterally wider (and proximodistally shorter) trochlea, a higher lateral rim, a steeper fibular facet (in which only the base is laterally protruding), a shallower groove for the flexor fibularis and a less developed posterior lateral tubercle, a more concave and shorter posterior calcaneal facet, a deeper sulcus tali, and a larger talar head. IPS85037 is projected onto intermediate scores, overlapping with platyrrhines, which indicates that its locomotor behavior likely included moderate amounts of quadrupedalism and climbing/clambering, and only a moderate proportion of suspensory behaviors. In contrast, KMN-RU 2036 displays very negative scores, close to the negative end of the axis, suggesting that its locomotor repertoire was dominated by quadrupedalism.

The second axis (PLS2; Figure 5B) discriminates the larger-bodied great apes on positive scores, thus being associated with slower-paced locomotion involving climbing, clambering, and suspensory movements, but completely lacking leaping from the lightly built platyrrhines, cercopithecoids, and gibbons. These latter habitually engage in swifter movements—such as fast quadrupedal progressions, brachiation, and leaping. Siamangs, despite their relatively small body size—comparable to many male macaques, female baboons, and the larger platyrrhine species—exhibit more positive scores than other hylobatids, in agreement with their generally slower and less acrobatic locomotor behavior. Positive scores are associated with a stouter talar shape, a more marked wedging of the anterior part of the trochlea, a shorter (and semilunar-shaped) anterior calcaneal facet, and a shorter and more medially angled neck. Contrarily, negative scores are associated with a slenderer and more gracile talar shape, parallel trochlear rims, a proximodistally longer anterior calcaneal facet, and a longer and less medially angled neck. IPS85037 falls closer to siamangs and great apes, suggesting that it similarly engaged in slower and more cautious locomotion without leaping (not surprisingly, given its large BM) and with high amounts of climbing and clambering. In contrast, KMN-RU 2036 (in accordance with its smaller BM) is located in more negative scores, overlapping with some of the larger-sized platyrrhines and cercopithecoids, which suggests a more agile locomotion (compatible with some degree of leaping) with less climbing/clambering than IPS85037 as well as extant great apes and siamangs.

The estimated locomotor repertoire for the hominoid to which IPS85037 belonged (Figure 6 and Table 8) includes large percentages of vertical climbing/clambering (CL = 50%) and quadrupedalism (QWR = 32%), and a comparatively restricted suspensory component (S = 11%). This locomotor profile, characterized by higher amounts of vertical climbing/clambering and quadrupedalism but lacking substantial suspensory behaviors, approaches the condition of two extant species: *Alouatta seniculus* (QWR = 46%; CL = 41%; S = 10%) and *Pan paniscus* (QWR = 36%; CL = 51%; S = 9%). In contrast, KMN RU 2036 is reconstructed as possessing a remarkably different locomotor repertoire, dominated by quadrupedalism (QWR = 81%), and with much lower percentages of vertical climbing/clambering (CL = 9%) and suspension (S = 2%).
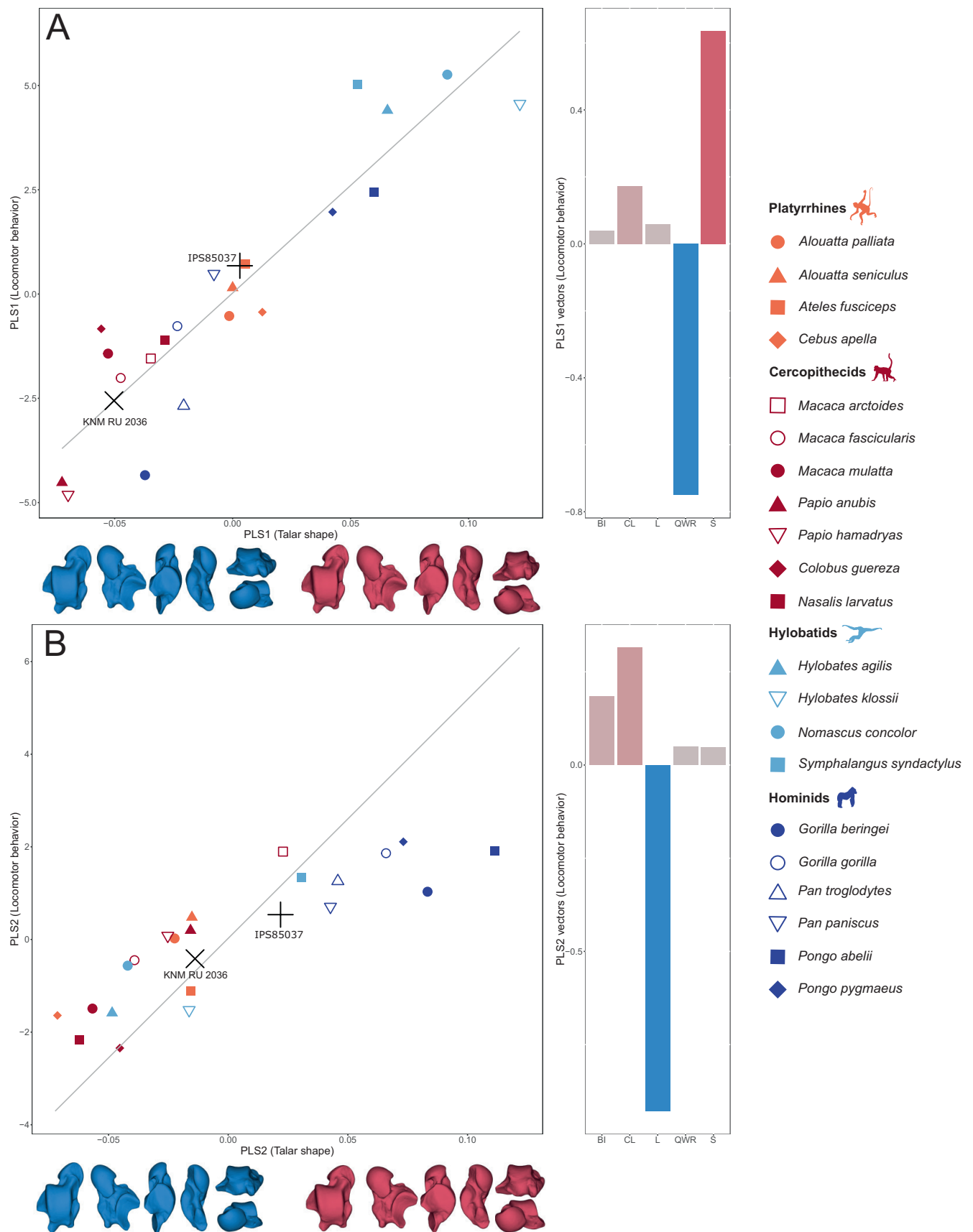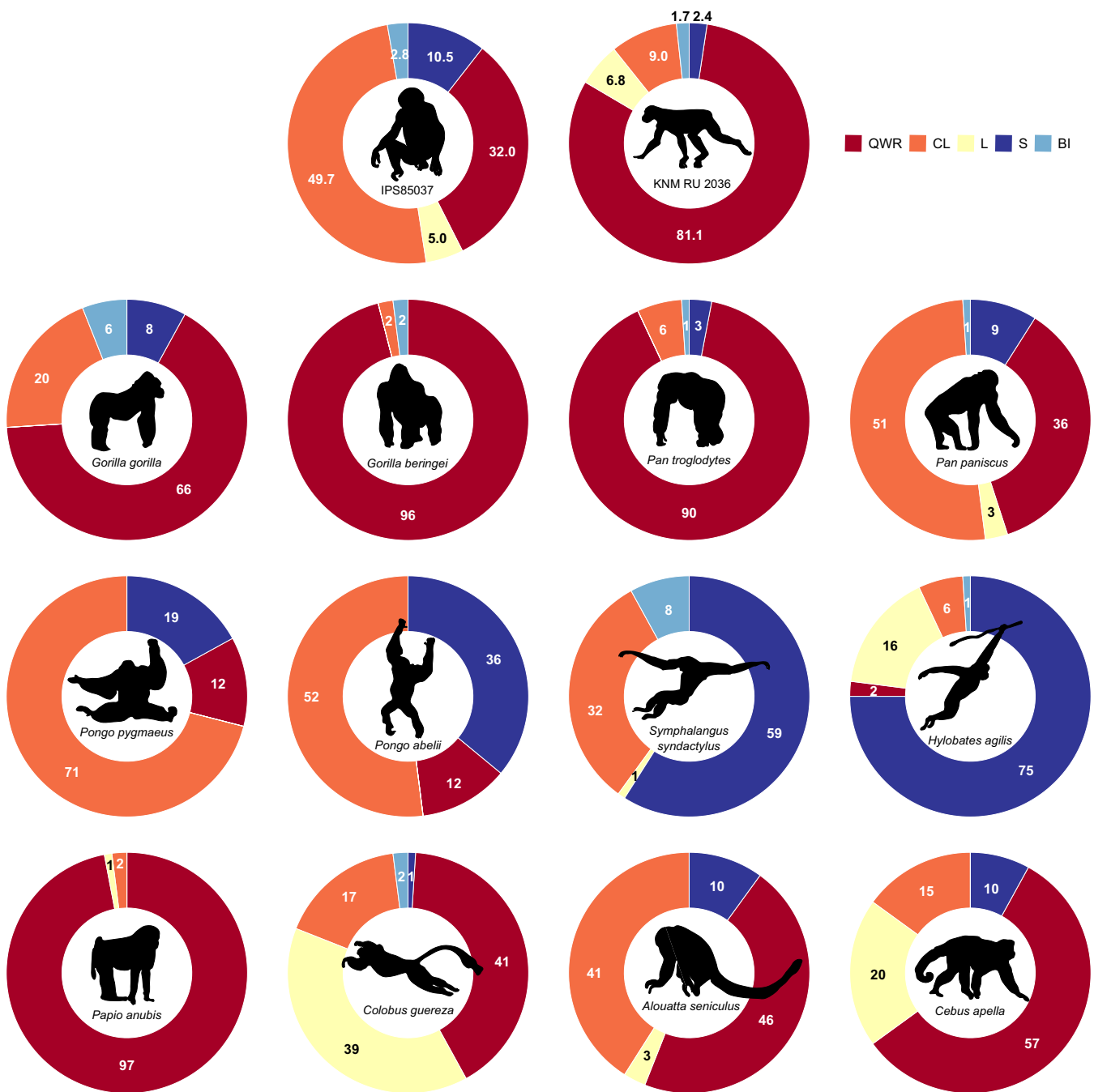
FIGURE 5 | Legend on next page.

FIGURE 6 | Donut charts summarizing the estimated locomotor repertoires of the Dryopithecini indet (IPS85037) and *Ekembo heseloni* (KMN RU 2036), as well as representatives of the main anthropoid groups from the extant comparative sample (Table S6). BI = bipedal walking; CL = clambering, and vertical climbing; L = leaping, dropping, and hopping; QWR = quadrupedal walking, bounding, and running; S = bridging, brachiation, and suspensory locomotion.

FIGURE 5 | Results of the two-block partial least squares for the first (PLS1; A) and second (PLS2; B) set of linear combinations between the species-mean Procrustes-aligned coordinates quantified locomotor data. The vectors of the first (A) or second (B) PLS axis of the locomotor variables (LMPs) are plotted to the right of each scatterplot. The groups distinguished a priori are color-coded, and each species is denoted by different symbols, as indicated in the legend. Fossil specimens (whose scores are projected a posteriori) are indicated by a cross (✕) sign (KMN RU 2036) and a plus (+) sign (IPS85037). Talar shape associated and magnified 3 times with minimum (blue) and maximum (red) values of covariation are plotted below each scatterplot (dorsal, plantar, lateral, medial, proximal, and distal views are shown, from left to right). Thin-plate spline warps are based on a talus of *Pan paniscus* (RMCA 27698). BI = bipedal walking; CL = clambering, and vertical climbing; L = leaping, dropping, and hopping; QWR = quadrupedal walking, bounding, and running; S = bridging, brachiation, and suspensory locomotion.

The PCA carried out on the locomotor percentages of the extant primate species distributes taxa according to their locomotor repertoire (Figure 7; Table S11). The first axis (PC1), which accounts for 41% of the total variance, discriminates quadrupedal species (platyrrhines, cercopithecoids, and African apes; most negative scores) from suspensory ones (orangutans and hylobatids; most positive scores). The second axis (PC2), which accounts for 26% of the total variance, separates those species with some leaping capabilities (including several platyrrhines, cercopithecoids and hylobatids, except for the larger-bodied siamangs; most positive scores) from those taxa with a more proclivity for climbing/clambering locomotion and lacking leaping behaviors (*Alouatta*, siamangs, and great apes; most negative scores). IPS85037 is projected closer to *Pan paniscus* and *Alouatta seniculus*, whereas the mainly quadrupedal locomotor repertoire estimated for KMN-RU 2036 overlaps with the more quadrupedal extant species.

TABLE 8 | Estimated locomotor percentages for IPS85037 and KMN RU 2036 using talar shape as a predictor.
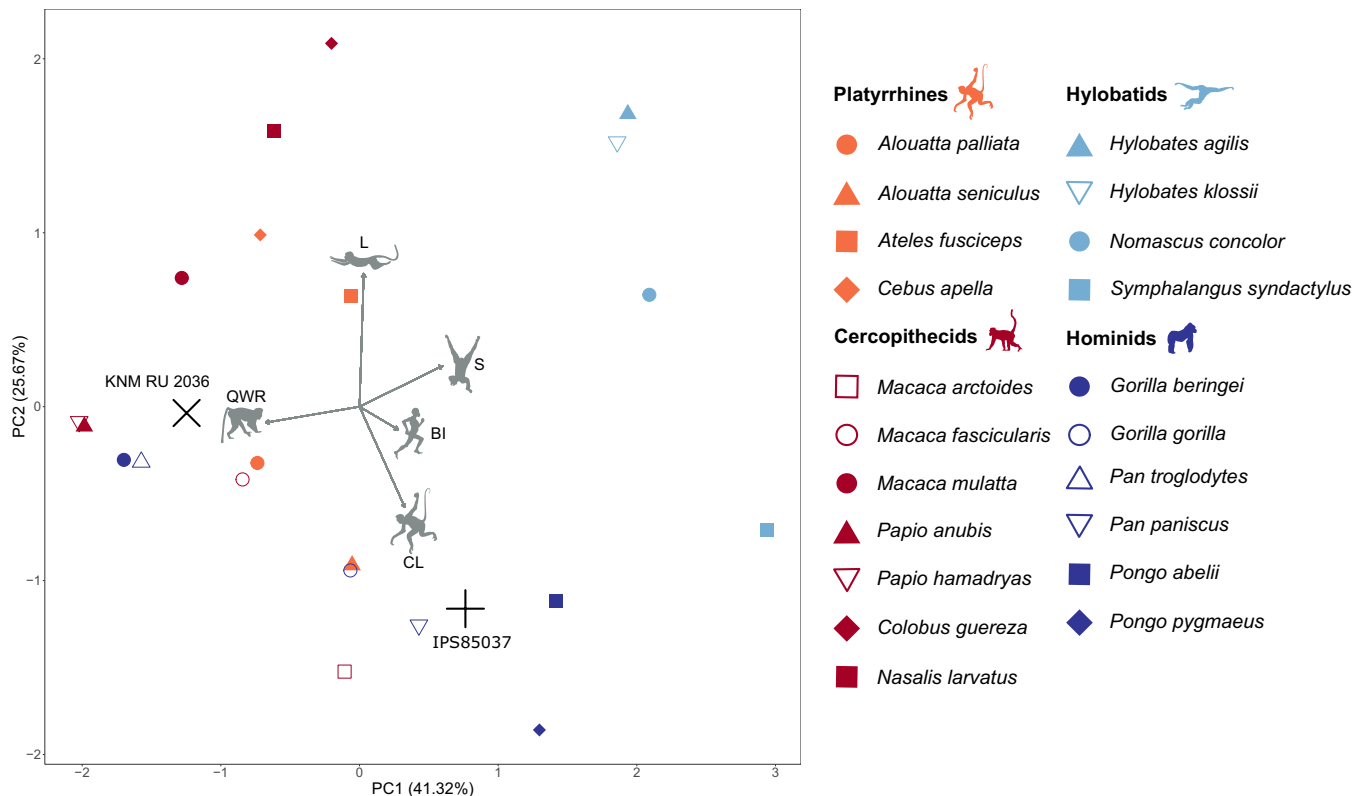
	QWR	CL	L	S	BI
IPS85037	32.0	49.7	5.0	10.5	2.8
KNM RU 2036	81.1	9.0	6.8	2.4	1.7

Abbreviations: BI = bipedal walking; CL = clambering and vertical climbing; L = leaping, dropping, and hopping; QWR = quadrupedal walking, bounding, and running; S = bridging, brachiation, and suspensory locomotion.

4 | Discussion

4.1 | Body Size, Sex Assignment, and Taxonomic Attribution

The talus IPS85037 displays several modern hominoid-like features (such as a wedge-shaped trochlea, broader anteriorly than posteriorly, well-developed posterior tubercles, an only slightly concave depression for the medial malleolus, a relatively flat, elongate and obliquely oriented posterior calcaneal facet and a medially angled talar neck) despite an overall "monkey-like" appearance (Harrison 1982; Langdon 1986; Gebo 1989; Drapeau 2022). This fact, coupled with its large body size, supports its attribution to a dryopithecine instead of any of the small-bodied catarrhines (*Pliopithecus* and *Pliobates*) recorded at ACM (Alba, Moyà-Solà et al. 2010, 2012; Alba et al. 2015; Bouchet et al. 2024). The estimated BM IPS85037 (~38 kg) is close to the average BM of female orangutans (Smith and Jungers 1997) and only slightly lower than estimates previously derived for other Vallès-Penedès dryopithecines: ~43 kg for *P. catalaunicus* from ACM/BCV1 (~12.0 Ma; Alba et al. 2022), based on a lumbar vertebra of the male holotype individual (Susanna et al. 2014); ~44 kg for *D. fontani* from ACM/C3-Az (~11.9 Ma; Alba et al. 2022), based on an isolated femur (Moyà-Solà, Köhler, et al. 2009); and ~39–40 kg for the male skeleton of *Hispanopithecus laietanus* from Can Llobateres 2 (~9.6 Ma; Casanovas-Vilar, Garcés, et al. 2016), based on vertebral and femoral measurements (Moyà-Solà et al. 2004; Moyà-Solà,

FIGURE 7 | Results of the principal components analysis (PCA) based on locomotor variables (LMPs) estimated for the fossil specimens as summarized by a bivariate plot of the first two PCs. The groups distinguished a priori are color-coded, and each species is denoted by different symbols, as indicated in the legend. Fossil specimens (whose scores are projected a posteriori) are indicated by a cross (✕) sign (KMN RU 2036) and a plus (+) sign (IPS85037). The vectors of each locomotor variable are projected as gray arrows. BI = bipedal walking; CL = clambering and vertical climbing; L = leaping, dropping, and hopping; QWR = quadrupedal walking, bounding, and running; S = bridging, brachiation, and suspensory locomotion.

Köhler, et al. 2009; Susanna et al. 2014). These estimates indicate that Vallès-Penedès male dryopithecines were generally slightly smaller on average than extant male chimpanzees. Thus, although IPS85037 more closely resembles the average female body mass of orangutans, given the usually marked sexual size dimorphism of Miocene apes (Schrein 2006; Scott et al. 2009), roughly comparable to that of extant orangutans (with males about twice the size of females), attributing IPS85037 to a female individual would imply a BM of ~75 kg, much larger than previously recorded for any Vallès-Penedès hominoid. Therefore, based on the estimated BM, we conclude that IPS85037 most probably belonged to a male specimen.

With an estimated age of ~11.7 Ma, IPS85037 represents one of the two latest occurrences of dryopithecins at ACM, postdating the latest record of the small-bodied pliopithecid *Pliopithecus canmatensis*, and minimally predating that of the crouzeliid *Pliobates cataloniae* (Alba et al. 2017, 2022; DeMiguel et al. 2021). The lack of associated craniodental material, together with the fact that the talus is not recorded for any of the ACM dryopithecins, make it impossible to attempt a taxonomic assignment to genus rank. However, based on both body size (see above) and chronology, IPS85037 might belong to any of the dryopithecins recorded from slightly older deposits along the ACM stratigraphic sequence—*P. catalaunicus, A. brevirostris,* and *D. fontani* (Moyà-Solà et al. 2004; Moyà-Solà, Köhler, et al. 2009; Moyà-Solà, Alba, et al. 2009; Alba et al. 2013, 2020; Alba, Bouchet, et al. 2024)—which overall range from ~12.4 to 11.9 Ma (Alba et al. 2017, 2022). To our knowledge, IPS85037 is the first complete dryopithecine talus described in detail— the talus originally attributed to *Rudapithecus hungaricus* by Morbeck (1983) was subsequently reassigned to the pliopithecoid *Anapithecus* by Kordos and Begun (2001), while only an undescribed partial talus (RUD 135) is seemingly attributable to *R. hungaricus* (Begun 2002, 2009). For this reason, even if no genus attribution is warranted, the quantitative comparisons between IPS85037 and the tali of extant anthropoids and the stem hominoid *E. heseloni* (KMN-RU 2036), as well as the morphological comparisons with other recovered Miocene ape and stem catarrhine tali, provide invaluable insight into the locomotor repertoire of Miocene dryopithecines as well as for the evolution of crown-hominoid locomotion.

4.2 | Morphofunctional Inferences and Quantitative Comparisons With Extant Anthropoids

The morphology of IPS85037, as it is frequently the case of Miocene ape morphology (e.g., Moyà-Solà et al. 2004; Pugh et al. 2023), displays a mosaic of features that is unknown among extant anthropoids, combining an overall plesiomorphic appearance as compared with extant apes with some traits that more closely resemble the derived talar morphology of modern hominoids (Harrison 1982; Conroy and Rose 1983; Drapeau 2022). Among plesiomorphic traits, the possession of a dorsoplantarly high talar body along with a relatively deep trochlea suggests less conjunct rotation (adduction and abduction) at the talocrural joint during dorsi- and plantarflexion, indicating that the movement occurring at the upper ankle joint is mostly limited at the parasagittal plane (Langdon 1986; Ward 1998).

Likewise, having an anteromedially L-shaped anterior calcaneal facet (resembling non-hominoid primates) has been associated with more limited inversion capabilities at the subtalar joint (Lewis 1980b)—contrasting with the crescent-shaped facet of extant hominoids, which has been related to increased inversion capabilities (Szalay and Langdon 1986).

Other features of IPS85037 that appear derived toward the crown hominoid condition are functionally related to high ranges of foot mobility and more powerful hallucal grasping (Langdon 1986; Drapeau 2022). For instance, IPS85037 resembles extant hominoids (particularly orangutans and hylobatids) in the possession of a more symmetrical trochlea, with a lateral rim that is only slightly dorsoplantarly higher than the medial one (Langdon 1986). The functional significance of this character is unclear, although it has been suggested that the presence of a prominent lateral rim might increase the amount of abduction accompanying the dorsiflexion of the foot (Strasser 1988). This, in turn, may be related to effective weight transfer during inversion and favor arboreal behavior, as concluded from studies performed in extant catarrhines (Turley and Frost 2013; Dunn et al. 2014; Knigge et al. 2015). However, it is noteworthy that this feature is more marked in terrestrial cercopithecines and African apes than in more arboreal cercopithecines, colobines, and Asian apes, suggesting a possible relationship with the use of terrestrial and/or larger horizontal substrates—as an adaptation for foot stabilization during walking and running, by limiting foot abduction and maintaining the foot in the parasagittal plane (Langdon 1986). The anterior widening of the trochlea in IPS85037 may be related to dorsiflexion during vertical climbing by facilitating the close packing of the talocrural joint as in extant great apes (Conroy and Rose 1983; Langdon 1986; DeSilva 2008, 2009). Posteriorly, the groove for the flexor hallucis longus tendon and the moderate development of the lateral (which serves as the attachment of the posterior talofibular ligament) and medial (which increases the load of the m. flexor hallucis longus) posterior tubercles are variably present among Miocene apes and stem catarrhine tali (Harrison 1982; Drapeau 2022). Judging by the depth of the groove and the moderate development of the lateral posterior tubercle, which acts as the insertion of the posterior talofibular ligament (an important ankle stabilizer during dorsiflexion; Leardini et al. 2000), IPS85037 is inferred to have possessed a powerful hallucal grasping, resembling extant African apes and suggesting frequent use of vertical climbing (DeSilva 2008). A strong hallucal grasp is inferred in other Miocene apes as well (Harrison 1982; Langdon 1986; Ward et al. 1993; Dunsworth 2006). On the medial side, IPS85037 displays only a slightly concave facet for articulation with the medial malleolus of the tibia that does not project medially, contrary to the close-packed configuration during dorsiflexion found in cercopithecoids (Le Gros Clark and Leakey 1951; Conroy and Rose 1983; Harrison 1986). This suggests an ankle adapted for withstanding large loadings during extreme dorsiflexion (DeSilva 2008). Similarly, the lack of a dorsal ridge on the talar neck, which is inferred to act as a locking mechanism for stopping the tibia during dorsiflexion, further indicates an ankle with a mobile talocrural joint (Le Gros Clark and Leakey 1951; Harrison 1982).

The possession of an elongated talar neck, normally considered the plesiomorphic condition for anthropoids, has been

hypothesized to be driven by allometric effects (Harrison 1982). However, this explanation does not apply to IPS85037, given its great ape-like BM. Orangutans also display a considerably elongated talar neck so that the talar head is projected further than the calcaneus, increasing the supination capability at the midtarsal joint during arboreal locomotion (Harrison 1982; Gebo 1989). The relatively deep groove for the flexor hallucis longus tendon in IPS85037 suggests that the calcaneus of the same individual, as in orangutans, was not distally elongated, implying a similarly high degree of midtarsal supination. In addition, the talar neck of IPS85037 also exhibits a very marked medial angulation, which is functionally related to the transmission of the compressive forces toward the medial side of the foot, occurring in arboreal animals with strong hallucal grasping (Barnett 1955; Harrison 1982). The spherical shape of the talar head in IPS85037 (similar to that of orangutans in size but somewhat smaller than that of cercopithecoids and African apes) and the great extent of the lateral side of the head (associated with better eversion capabilities of the forefoot) indicate that IPS85037 lacks the typical dorsal translation of the navicular observed in extant apes and would have been less capable of coping with large compressive forces than extant hominoids (Szalay and Langdon 1986; Meldrum and Wunderlich 1998). In turn, the posterior calcaneal facet, which is shallow and gently curved (resembling that of orangutans), indicates greater laxity and mobility at this joint, associated with better inversion capabilities at the subtalar joint (Gomberg 1981; Langdon 1986; Yapuncich and Granatosky 2021). Finally, IPS85037 exhibits a small divergence between the posterior calcaneal facet and the long axis of the trochlea, facilitating the screw motion of the talus at the level of the subtalar joint and enhancing the inversion of the foot (Conroy and Rose 1983).

The predicted LMPs for IPS85037 using the 2B-PLS regression models indicate a locomotor repertoire dominated by vertical climbing/clambering and quadrupedalism, with some degree of suspension. In contrast, the LMPs predicted for KMN RU 2036 indicate a very different locomotor repertoire, vastly dominated by quadrupedalism and with only small amounts of vertical climbing/clambering. These estimated percentages cannot be taken at face value because they are based on a single bone, although the errors computed for the extant species are not particularly large, indicating that the talus is a reliable predictor for locomotor behavior. Furthermore, the results for KMN RU 2036—which match the locomotor profile of some colobine monkeys and non-atelid platyrrhines (Youlatos and Meldrum 2011; Hunt 2016)—are consistent with previous locomotor inferences for *Ekembo* based on its postcranial morphology (Le Gros Clark 1952; Conroy and Rose 1983; Rose 1983, 1988; Gebo et al. 1988, 2009; Ward 1993, 1997; Ward et al. 1995; Walker 1997; Dunsworth 2006; DeSilva 2008). The combination of locomotor modes estimated for IPS85037 approaches that of two extant species: *Alouatta seniculus* and *Pan paniscus*. The former seems to be the species that exhibits the highest percentages of clambering/climbing among atelids (and platyrrhines in general; Youlatos and Meldrum 2011), which has been related to the diversity of habitats exploited by this species (including gallery forests and different types of shrub woodlands; Schön Ybarra and Schön 1987). In turn, bonobos are the most generalized great apes in terms of locomotion (Doran 1993; Isler 2002; Ramos 2014). This is reflected by their pedal anatomy, which

combines features related to high foot mobility (e.g., comparatively subequal lateral and medial talar rims, slightly concave posterior calcaneal facet, mediolaterally broad anterior calcaneal facet) and propulsion (such as relatively large heel to provide lever arm; Vereecke et al. 2005; Friesen et al. 2024). Compared to orangutans, which exhibit a slow and cautious locomotion dominated by orthograde clambering and forelimb-dominated suspension (Cant 1987; Manduell et al. 2011), bonobos engage much less frequently in suspensory behaviors and equally divide their time between the forest floor and the arboreal canopy (Ramos 2014). Similarly, to chimpanzees and gorillas, bonobos spend a great amount of their time on the ground, habitually moving quadrupedally using knuckle-walking, which is an unlikely behavior for IPS85037 based on the hand morphology of dryopithecines (Almécija et al. 2009; Alba, Almécija, et al. 2010). However, bonobos also engage in more arboreal quadrupedalism than chimpanzees, being primarily palmigrade (Doran 1993), a type of locomotor mode that was likely used by most Miocene apes to varying degrees (Rose 1994; Almécija et al. 2007, 2021, 2009; Alba, Almécija, et al. 2010, 2012; Alba 2012; Ward 2015). Moreover, the morphology of several pedal elements of bonobos (including the talus and the medial cuneiform) suggests that they possess a greater range of hallucal abduction compared to other African apes, offering an advantage for maintaining strong pedal grips while climbing more varied and smaller arboreal substrates (Friesen et al. 2024). Remarkably, some talar features of bonobos, providing them with greater versatility at the ankle and subtalar joints (such as the even lateral and medial trochlear rims and the slightly concave posterior calcaneal facet), are also present in IPS85037.

4.3 | Implications for the Evolution of Crown Hominoid Positional Behaviors

The feet of extant apes display increased mobility and prehensility as compared with those of other living anthropoids, in agreement with the more varied and non-stereotypical locomotor behaviors of the former, which may be interpreted as an adaptation for navigating across precarious and unpredictably oriented arboreal substrates (Conroy and Rose 1983; Hunt 1991, 2016; DeSilva 2008; Drapeau 2022). In accordance with this, extant ape tali are distinguished by numerous adaptations related to enhanced stability during inversion and dorsiflexion, accommodating the foot into different positions and providing strong anchorage to the substrate (Conroy and Rose 1983; Langdon 1986; Strasser 1988; Gebo 1989; Parr et al. 2014; Drapeau 2022). However, almost all recovered tali of different groups of Miocene apes and stem catarrhines (pliopithecoids and dendropithecids) lack evidence of a specialized modern hominoid-like derived morphology and, in most cases, exhibit remarkable morphological uniformity (Harrison 1982; Conroy and Rose 1983; Rose 1994; Drapeau 2022).

Talar morphology of stem catarrhines (e.g., pliopithecoids and dendropithecids) evinces a foot more adapted to stable dorsiflexion and inversion than earlier stem anthropoids (such as parapithecoids, oligopithecoids, and propliopithecoids; Fleagle 1980; Fleagle and Simons 1983, 1995; Gebo and Simons 1987; Seiffert and Simons 2001) and extant cercopithecoids and non-suspensory platyrrhines, as indicated by the possession of a mediolaterally

broad talar head, although they still retain an overall plesiomorphic appearance, exemplified by their trochlear proportions, lack of lateral flaring of the fibular facet, and proximodistally elongated talar neck (Le Gros Clark and Thomas 1951; Harrison 1982; Rose et al. 1992). Consequently, they are reconstructed as arboreal quadrupeds with, in some cases, moderate climbing and suspensory capabilities, resembling extant atelids in some respects (Harrison 1982; Sarmiento 1983; Rose 1988, 1994; Rose et al. 1992; Alba et al. 2015; Arias-Martorell et al. 2015; Arias-Martorell et al. 2021). Stem hominoids overall still display a very plesiomorphic talar morphology, although they already exhibit some other derived hominoid-like features (e.g., a fibular facet that flares more laterally), indicating a foot better adapted for grasping supports in a greater variety of positions than earlier stem catarrhines (Conroy and Rose 1983; Walker 1997; Dunsworth 2006). For instance, proconsulids (*Proconsul* and *Ekembo*), despite their vastly disparate range of BM (from *Pr. africanus* and *E. heseloni*, estimated between 9 and 15 kg, to *Pr. major*, with a body mass around 60–90 kg, comparable to a female *Gorilla*; Harrison 1982; Rafferty et al. 1995), are reconstructed as primarily arboreal quadrupeds that engaged in some climbing and pronograde clambering, assisted by a strong hallux adapted to powerful grasping (Walker 1997; Ward 2015). Our estimated locomotor percentages for KMN RU 2036 (*E. heseloni*) are consistent with this view, obtaining a locomotor repertoire with a large quadrupedal component, little (but not insignificant) climbing and clambering, and a lack of suspensory behaviors. Only the largest species, *Pr. major*, exhibits some talar features (e.g., deep groove for the flexor hallucis longus, developed lateral and medial posterior tubercles), as well as other postcranial adaptations, suggesting a higher proclivity for vertical climbing and other antipronograde behaviors (DeSilva 2008). Other stem hominoids, such as the afropithecids *Eq. africanus* and *N. kerioi*, provide further evidence that a broad plesiomorphic appearance, except for some derived hominoid-like features (e.g., fibular facet that flares more laterally, mediolaterally expanded talar head), characterized ape talar morphology during the Early/Middle Miocene (McCrossin 1994; Rose et al. 1996; Ishida et al. 2004; Nakatsukasa et al. 2012).

Compared to earlier Miocene ape and stem catarrhine tali, IPS85037 appears to be more derived toward the extant hominoid condition in features associated with greater mobility at the talocrural joint (a relatively wedged trochlea, subequal talar rims, the lack of a dorsal tubercle on the neck, a less concave articular basin for the medial tibial malleolus), subtalar joint (a slightly angled, proximodistally elongated and shallow posterior calcaneal facet), and greater prehensility (a deep groove for the m. flexor hallucis longus tendon, a developed and prominent lateral posterior tubercle, and a medially angled talar neck). However, the overall gracile appearance of IPS85037, emphasized by the relatively elongated neck and the small head, as well as several plesiomorphic features (relatively deep trochlear groove, an L-shaped anteromedially located anterior calcaneal facet, a laterally extended articular facet for the navicular on the talar head) reveal that, independently of the acquisition of an orthograde body plan and a more forelimb-dominated locomotion, the structure of the foot remained relatively generalized during most of hominoid evolution, with only changes for increased mobility and stronger hallucal grasping but lacking clear-cut adaptations for suspensory behavior. A similar mosaic

pattern is observed in the slightly younger stem pongine *Si. sivalensis*, revealing that the talocrural and subtalar joints had more limited inversion/eversion capabilities than in extant hominoids, but greater than in cercopithecoids (Pilbeam et al. 1980; Madar 1996). In contrast, the Late Miocene stem hominoid *O. bambolii* exhibits a uniquely derived hominoid-like talar morphology among Miocene apes (Szalay and Langdon 1986), which, together with other postcranial adaptations, has been associated with a wide array of antipronograde behaviors, including vertical climbing and suspension (Jungers 1987; Russo and Shapiro 2013; Hammond et al. 2020).

The mosaic morphology of IPS85037 concurs with the pattern combining plesiomorphic and crown hominoid-like derived traits exhibited by other anatomical regions attributed to the Vallès-Penedès dryopithecines, particularly *Pierolapithecus* (Moyà-Solà et al. 2004, 2005; Almécija et al. 2009; Alba, Almécija, et al. 2010; Hammond et al. 2013; Pina et al. 2014; Pina et al. 2020) and *Dryopithecus* (Moyà-Solà, Köhler, et al. 2009; Alba et al. 2011; Almécija et al. 2012; Pina et al. 2019), but also to a lesser extent *Hispanopithecus* (Moyà-Solà and Köhler 1996; Almécija et al. 2007; Alba, Almécija, et al. 2012; Tallman et al. 2013; Susanna et al. 2014). Regardless of the exact phylogenetic position of dryopithecines, either as stem hominids (Andrews 1992; Casanovas-Vilar et al. 2011; Alba 2012; Alba et al. 2015; Pugh 2022) or more closely related to pongines (Moyà-Solà and Köhler 1993, 1995, 1996; Agustí et al. 1996) or hominines (Begun 2002, 2009, 2015, 2018; Begun et al. 2012), the morphology and estimated locomotor repertoire of IPS85037 reinforce the numerous evidence (e.g., Tuttle 1975; Larson 1998; Alba 2012; Almécija et al. 2021) that adaptations for suspensory locomotion and an orthograde body plan did not evolve at the same time, but rather were acquired independently in different lineages during hominoid evolution.

5 | Conclusions

An isolated primate talus (IPS85037) from ACM dated to ~11.7 Ma (close to the Middle/Late Miocene boundary) is described and compared with a sample of extant anthropoids as well as the stem hominoid *E. heseloni* (KMN RU 2036). Body mass estimates based on talar size (close to a female orangutan) and the possession of some derived modern hominoid features suggest that the specimen belongs to a male dryopithecine, but an attribution to genus rank is precluded by the lack of comparative material. Talar shape, quantified by means of 3DGM, indicates that IPS85037 displays a mosaic of plesiomorphic and apomorphic features relative to crown hominoids, unknown among modern anthropoids but resembling other Miocene ape tali. Compared to KMN RU 2036, IPS85037 presents several characters associated with relatively more mobile talocrural and subtalar joints and evidence of strong hallucal grasping. This is confirmed by the locomotor repertoire inferred from the covariation between talar shape and locomotor percentages, which indicate important quadrupedal and clambering/climbing components but much more restricted suspensory behaviors. Within extant species, *Alouatta seniculus* and *Pan paniscus* concur the most with this locomotor repertoire. In contrast, locomotor estimations based on KMN RU 2036 shape indicate a locomotor repertoire vastly dominated by quadrupedalism, resembling extant

cercopithecoids. Both the morphology and locomotor repertoire inferred for IPS85037 are broadly consistent with previous inferences for the Middle Miocene dryopithecins *Pierolapithecus* and, to a lesser extent, *Dryopithecus* but differ from the greater emphasis on suspensory behaviors displayed by the younger hispanopithecins *Hispanopithecus*, *Danuvius*, and *Rudapithecus*.

Author Contributions

Oriol Monclús-Gonzalo: conceptualization (equal), formal analysis (lead), investigation (lead), methodology (supporting), writing – original draft (lead), writing – review and editing (supporting). **Shubham Pal:** formal analysis (supporting), investigation (supporting), writing – original draft (supporting). **Thomas A. Püschel:** methodology (lead), writing – review and editing (supporting). **Alessandro Urciuoli:** methodology (supporting), writing – review and editing (supporting). **Víctor Vinuesa:** data curation (supporting), methodology (supporting). **Josep M. Robles:** data curation (lead). **Sergio Almécija:** conceptualization (equal), data curation (equal), methodology (supporting), resources (lead), supervision (supporting), writing – review and editing (supporting). **David M. Alba:** conceptualization (equal), funding acquisition (lead), supervision (lead), writing – original draft (supporting), writing – review and editing (lead).

Data Availability Statement

The described original fossil is available for study from the ICP, which is a registered museums recognized by the Generalitat de Catalunya, while its digital 3D model is available from MorphoSouce (https://doi.org/10.17602/M2/M713734). 3D landmark coordinates used in this study are openly available in figshare (https://figshare.com/s/fcc3e39fee03117ed06f).

References

Adams, D. C., and E. Otárola-Castillo. 2013. "Geomorph: An R Package for the Collection and Analysis of Geometric Morphometric Shape Data." *Methods in Ecology and Evolution* 4, no. 4: 393–399. https://doi.org/10.1111/2041-210X.12035.

Adler, D., and D. Murdoch. 2020. "Rgl: 3D Visualization Using openGL." https://github.com/dmurdoch/rgl. https://dmurdoch.github.io/rgl/.

Agustí, J., M. Köhler, S. Moyà-Solà, L. Cabrera, M. Garcés, and J. M. Parés. 1996. "Can Llobateres: The Pattern and Timing of the Vallesian Hominoid Radiation Reconsidered." *Journal of Human Evolution* 31, no. 2: 143–155. https://doi.org/10.1006/jhev.1996.0055.

Alba, D. M. 2012. "Fossil Apes From the Vallès-Penedès Basin." *Evolutionary Anthropology* 21: 254–269. https://doi.org/10.1002/evan.21312.

Alba, D. M., S. Almécija, I. Casanovas-Vilar, J. M. Méndez, and S. Moyà-Solà. 2012. "A Partial Skeleton of the Fossil Great Ape *Hispanopithecus laietanus* From Can Feu and the Mosaic Evolution of Crown-Hominoid

Positional Behaviors." *PLoS One* 7: e39617. https://doi.org/10.1371/journal.pone.0039617.

Alba, D. M., S. Almécija, D. DeMiguel, et al. 2015. "Miocene Small-Bodied Ape From Eurasia Sheds Light on Hominoid Evolution." *Science* 350: aab2625. https://doi.org/10.1126/science.aab2625.

Alba, D. M., S. Almécija, and S. Moyà-Solà. 2010. "Locomotor Inferences in *Pierolapithecus* and *Hispanopithecus*: Reply to Deane and Begun (2008)." *Journal of Human Evolution* 59: 143–149. https://doi.org/10.1016/j.jhevol.2010.02.002.

Alba, D. M., F. Bouchet, J. Fortuny, et al. 2024. "New Remains of the Miocene Great Ape *Anoiapithecus brevirostris* From Abocador de Can Mata." *Journal of Human Evolution* 188: 103497. https://doi.org/10.1016/j.jhevol.2024.103497.

Alba, D. M., I. Casanovas-Vilar, M. Garcés, and J. M. Robles. 2017. "Ten Years in the Dump: An Updated Review of the Miocene Primate-Bearing Localities From Abocador de Can Mata (NE Iberian Peninsula)." *Journal of Human Evolution* 102: 12–20. https://doi.org/10.1016/j.jhevol.2016.09.012.

Alba, D. M., E. Delson, G. Carnevale, et al. 2014. "First Joint Record of *Mesopithecus* and cf. *Macaca* in the Miocene of Europe." *Journal of Human Evolution* 67: 1–18. https://doi.org/10.1016/j.jhevol.2013.11.001.

Alba, D. M., J. Fortuny, M. Pérez de los Ríos, et al. 2013. "New Dental Remains of *Anoiapithecus* and the First Appearance Datum of Hominoids in the Iberian Peninsula." *Journal of Human Evolution* 65: 573–584. https://doi.org/10.1016/j.jhevol.2013.07.003.

Alba, D. M., J. Fortuny, J. M. Robles, et al. 2020. "A New Dryopithecine Mandibular Fragment From the Middle Miocene of Abocador de Can Mata and the Taxonomic Status of 'Sivapithecus' occidentalis From Can Vila (Vallès-Penedès Basin, NE Iberian Peninsula)." *Journal of Human Evolution* 145: 102790. https://doi.org/10.1016/j.jhevol.2020.102790.

Alba, D. M., and S. Moyà-Solà. 2012. "On the Identity of a Hominoid Male Upper Canine From the Vallès-Penedès Basin Figured by Pickford (2012)." *Estudios Geológicos* 68: 149–153. https://doi.org/10.3989/egeol.40900.180.

Alba, D. M., S. Moyà-Solà, and S. Almécija. 2011. "A Partial Hominoid Humerus From the Middle Miocene of Castell de Barberà (Vallès-Penedès Basin, Catalonia, Spain)." *American Journal of Physical Anthropology* 144: 365–381. https://doi.org/10.1002/ajpa.21417.

Alba, D. M., S. Moyà-Solà, I. Casanovas-Vilar, et al. 2006. "Los Vertebrados Fósiles del Abocador de Can Mata (els Hostalets de Pierola, l'Anoia, Cataluña), una Sucesión de Localidades del Aragoniense Superior (MN6 y MN7+8) de la Cuenca del Vallès-Penedès. Campañas 2002–2003, 2004 Y 2005." *Estudios Geológicos* 62, no. 1: 295–312. https://doi.org/10.3989/egeol.0662127.

Alba, D. M., S. Moyà-Solà, A. Malgosa, et al. 2010. "A New Species of *Pliopithecus* Gervais, 1849 (Primates: Pliopithecidae) From the Middle Miocene (MN8) of Abocador de Can Mata (Els Hostalets de Pierola, Catalonia, Spain)." *American Journal of Physical Anthropology* 141, no. 1: 52–75. https://doi.org/10.1002/ajpa.21114.

Alba, D. M., S. Moyà-Solà, J. M. Robles, and J. Galindo. 2012. "Brief Communication: The Oldest Pliopithecid Record in the Iberian Peninsula Based on New Material From the Vallès-Penedès Basin." *American Journal of Physical Anthropology* 147: 135–140. https://doi.org/10.1002/ajpa.21631.

Alba, D. M., J. M. Robles, I. Casanovas-Vilar, et al. 2022. "A Revised (Earliest Vallesian) age for the Hominoid-Bearing Locality of Can Mata 1 Based on New Magnetostratigraphic and Biostratigraphic Data From Abocador de Can Mata (Vallès-Penedès Basin, NE Iberian Peninsula)." *Journal of Human Evolution* 170: 103237. https://doi.org/10.1016/j.jhevol.2022.103237.

Alba, D. M., A. Urciuoli, A. S. Hammond, S. Almécija, L. Rook, and C. Zanolli. 2024. "Miocene Ape Evolution: Where Does *Oreopithecus* Fit

in?" *Bollettino della Societa Paleontologica Italiana* 63, no. 2: 153–182. https://doi.org/10.4435/BSPI.2024.01.

Almécija, S., D. M. Alba, and S. Moya-Sola. 2009. "*Pierolapithecus* and the Functional Morphology of Miocene Ape Hand Phalanges: Paleobiological and Evolutionary Implications." *Journal of Human Evolution* 57: 284–297. https://doi.org/10.1016/j.jhevol.2009.02.008.

Almécija, S., D. M. Alba, and S. Moyà-Solà. 2012. "The Thumb of Miocene Apes: New Insights From Castell de Barberà (Catalonia, Spain)." *American Journal of Physical Anthropology* 148: 436–450. https://doi.org/10.1002/ajpa.22071.

Almécija, S., D. M. Alba, S. Moyà-Solà, and M. Köhler. 2007. "Orang-Like Manual Adaptations in the Fossil Hominoid *Hispanopithecus laietanus*: First Steps Towards Great Ape Suspensory Behaviours." *Proceedings. Biological Sciences* 274, no. 1624: 2375–2384. https://doi.org/10.1098/rspb.2007.0750.

Almécija, S., A. S. Hammond, N. E. Thompson, K. D. Pugh, S. Moyà-Solà, and D. M. Alba. 2021. "Fossil Apes and Human Evolution." *Science* 372, no. 6542: eabb4363. https://doi.org/10.1126/science.abb4363.

Almécija, S., C. M. Orr, M. W. Tocheri, B. A. Patel, and W. L. Jungers. 2015. "Exploring Phylogenetic and Functional Signals in Complex Morphologies: The Hamate of Extant Anthropoids as a Test-Case Study." *Anatomical Record* 298: 212–229. https://doi.org/10.1002/ar.23079.

Andrews, P. 1992. "Evolution and Environment in the Hominoidea." *Nature* 360: 641–646. https://doi.org/10.1038/360641a0.

Archer, W., C. M. Pop, Z. Rezek, et al. 2018. "A Geometric Morphometric Relationship Predicts Stone Flake Shape and Size Variability." *Archaeological and Anthropological Sciences* 10: 1991–2003. https://doi.org/10.1007/s12520-017-0517-2.

Arias-Martorell, J., D. M. Alba, J. M. Potau, G. Bello-Hellegouarch, and A. Pérez-Pérez. 2015. "Morphological Affinities of the Proximal Humerus of *Epipliopithecus vindobonensis* and *Pliopithecus antiquus*: Suspensory Inferences Based on a 3D Geometric Morphometrics Approach." *Journal of Human Evolution* 80: 83–95. https://doi.org/10.1016/j.jhevol.2014.08.012.

Arias-Martorell, J., S. Almécija, A. Urciuoli, M. Nakatsukasa, S. Moyà-Solà, and D. M. Alba. 2021. "A Proximal Radius of *Barberapithecus huerzeleri* From Castell de Barberà: Implications for Locomotor Diversity Among Pliopithecoids." *Journal of Human Evolution* 157: 103032. https://doi.org/10.1016/j.jhevol.2021.103032.

Barnett, C. H. 1955. "Some Factors Influencing Angulation of the Neck of the Mammalian Talus." *Journal of Anatomy* 89: 225–230.

Bastir, M., N. Torres-Tamayo, C. A. Palancar, et al. 2019. "Geometric Morphometric Studies in the Human Spine." In *Spinal Evolution*, edited by E. Been, A. Gómez-Olivencia, and P. A. Kramer, 361–386. Springer. https://doi.org/10.1007/978-3-030-19349-2_16.

Begun, D. R. 1987. "A Review of the Genus *Dryopithecus*" (PhD diss., University of Pennsylvania).

Begun, D. R. 2002. "European Hominoids." In *The Primate Fossil Record*, edited by W. C. Hartwig, 339–368. Cambridge University Press.

Begun, D. R. 2009. "Dryopithecins, Darwin, de Bonis, and the European Origin of the African Apes and Human Clade." *Geodiversitas* 31: 789–816. https://doi.org/10.5252/g2009n4a789.

Begun, D. R. 2015. "Fossil Record of Miocene Hominoids." In *Handbook of Paleoanthropology*, edited by W. Henke and I. Tattersall, 1261–1332. Springer. https://doi.org/10.1007/978-3-642-39979-4_32.

Begun, D. R. 2018. "*Dryopithecus*." In *The International Encyclopedia of Biological Anthropology*, edited by W. Trevathan. John Wiley and Sons. https://doi.org/10.1002/9781118584538.ieba0143.

Begun, D. R., M. C. Nargolwalla, and L. Kordos. 2012. "European Miocene Hominids and the Origin of the African Ape and Human Clade." *Evolutionary Anthropology* 21: 10–23. https://doi.org/10.1002/evan.20329.

Begun, D. R., and C. V. Ward. 2005. "Comment on '*Pierolapithecus catalaunicus*, a New Middle Miocene Great Ape From Spain'." *Science* 208: 203c. https://doi.org/10.1126/science.1108139.

Böhme, M., N. Spassov, J. Fuss, et al. 2019. "A New Miocene Ape and Locomotion in the Ancestor of Great Apes and Humans." *Nature* 575: 489–493. https://doi.org/10.1038/s41586-019-1731-0.

Bookstein, F. L. 2019. "Pathologies of Between-Groups Principal Components Analysis in Geometric Morphometrics." *Evolutionary Biology* 46: 271–302. https://doi.org/10.1007/s11692-019-09484-8.

Bouchet, F., C. Zanolli, A. Urciuoli, et al. 2024. "The Miocene Primate *Pliobates* Is a Pliopithecoid." *Nature Communications* 15: 2822. https://doi.org/10.1038/s41467-024-47034-9.

Cant, J. G. 1987. "Positional Behavior of Female Bornean Orangutans (*Pongo pygmaeus*)." *American Journal of Primatology* 12: 71–90. https://doi.org/10.1002/ajp.1350120104.

Cardini, A., P. O'Higgins, and F. J. Rohlf. 2019. "Seeing Distinct Groups Where There Are None: Spurious Patterns From Between-Group PCA." *Evolutionary Biology* 46, no. 4: 303–316. https://doi.org/10.1007/s11692-019-09487-5.

Cardini, A., and P. D. Polly. 2020. "Cross-Validated Between Group PCA Scatterplots: A Solution to Spurious Group Separation?" *Evolutionary Biology* 47, no. 1: 85–95. https://doi.org/10.1007/s11692-020-09494-x.

Casanovas-Vilar, I., D. M. Alba, M. Garcés, J. M. Robles, and S. Moyà-Solà. 2011. "Updated Chronology for the Miocene Hominoid Radiation in Western Eurasia." *Proceedings of the National Academy of Sciences* 108: 5554–5559. https://doi.org/10.1073/pnas.1018562108.

Casanovas-Vilar, I., M. Garcés, J. A. van Dam, I. García Paredes, J. M. Robles, and D. M. Alba. 2016. "An Updated Biostratigraphy for the Late Aragonian and the Vallesian of the Vallès-Penedès Basin (Catalonia)." *Geologica Acta* 14: 195–217. https://doi.org/10.1344/GeologicaActa2016.14.3.1.

Casanovas-Vilar, I., S. Jovells-Vaqué, and D. M. Alba. 2022. "The Miocene High-Resolution Record of the Vallès-Penedès Basin (Catalonia)." In *NOW 25th Anniversary Meeting. Sabadell (Barcelona), 16–18 November 2022*, edited by I. Casanovas-Vilar and D. M. Alba, 79–122. Abstract Book & Fieldtrip Guide. Paleontol. Evol., Memòria Especial.

Casanovas-Vilar, I., A. Madern, D. M. Alba, et al. 2016. "The Miocene Mammal Record of the Vallès-Penedès Basin (Catalonia)." *Comptes Rendus Palevol* 15: 791–812. https://doi.org/10.1016/j.crpv.2015.07.004.

Collyer, M. L., and D. C. Adams. 2018. "RRPP: An R Package for Fitting Linear Models to High-Dimensional Data Using Residual Randomization." *Methods in Ecology and Evolution* 9, no. 7: 1772–1779. https://doi.org/10.1111/2041-210X.13029.

Conroy, G. C., and M. D. Rose. 1983. "The Evolution of the Primate Foot From the Earliest Primates to the Miocene Hominoids." *Foot & Ankle* 3: 342–364. https://doi.org/10.1177/107110078300300604.

Cramer, J. S. 2003. "The Origins and Developments of the Logit Model." In *Logit Models From Economics and Other Fields*, edited by J. S. Cramer, 149–158. Cambridge University Press. https://doi.org/10.1017/CBO9780511615412.010.

Culhane, A. C., G. Perriere, E. C. Considine, T. G. Cotter, and D. G. Higgins. 2002. "Between-Group Analysis of Microarray Data." *Bioinformatics* 18: 1600–1608. https://doi.org/10.1093/bioinformatics/18.12.1600.

Day, M. H., and B. A. Wood. 1968. "Functional Affinities of the Olduvai Hominid 8 Talus." *Man* 3, no. 3: 440–455. https://doi.org/10.2307/2798879.

Day, M. H., and B. A. Wood. 1969. "Hominoid Tali From East Africa." *Nature* 222: 591–592. https://doi.org/10.1038/222591a0.

Deane, A. S., and D. R. Begun. 2008. "Broken Fingers: Retesting Locomotor Hypotheses for Fossil Hominoids Using Fragmentary Proximal Phalanges and High-Resolution Polynomial Curve Fitting (HR-PCF)." *Journal of Human Evolution* 55: 691–701. https://doi.org/10.1016/j.jhevol.2008.05.005.

Deane, A. S., and D. R. Begun. 2010. "*Pierolapithecus* Locomotor Adaptations: A Reply to Alba et al.'s Comment on Deane and Begun (2008)." *Journal of Human Evolution* 59: 150–154. https://doi.org/10.1016/j.jhevol.2010.04.003.

DeMiguel, D., L. Domingo, I. M. Sánchez, I. Casanovas-Vilar, J. M. Robles, and D. M. Alba. 2021. "Palaeoecological Differences Underlie Rare Co-Occurrence of Miocene European Primates." *BMC Biology* 19: 6. https://doi.org/10.1186/s12915-020-00939-5.

DeSilva, J. M. 2008. "Vertical Climbing Adaptations in the Anthropoid Ankle and Midfoot: Implications for Locomotion in Miocene Catarrhines and Plio-Pleistocene Hominins" (PhD diss., University of Michigan).

DeSilva, J. M. 2009. "Functional Morphology of the Ankle and the Likelihood of Climbing in Early Hominins." *Proceedings of the National Academy of Sciences* 106: 6567–6572. https://doi.org/10.1073/pnas.0900270106.

Doran, D. M. 1993. "Comparative Locomotor Behavior of Chimpanzees and Bonobos: The Influence of Morphology on Locomotion." *American Journal of Physical Anthropology* 91: 83–98. https://doi.org/10.1002/ajpa.1330910106.

Drapeau, M. 2022. "Miocene Ape Feet." In *The Evolution of the Primate Foot*, edited by A. Zeininger, K. G. Hatala, R. E. Wunderlich, and D. Schmitt, 321–359. Springer. https://doi.org/10.1007/978-3-031-06436-4_13.

Dunn, R. H., M. W. Tocheri, C. M. Orr, and W. L. Jungers. 2014. "Ecological Divergence and Talar Morphology in Gorillas." *American Journal of Physical Anthropology* 153: 526–541. https://doi.org/10.1002/ajpa.22451.

Dunsworth, H. M. 2006. "*Proconsul heseloni* Feet From Rusinga Island, Kenya" (PhD diss., Pennsylvania State University).

Fabre, A. C., M. C. Granatosky, J. B. Hanna, and D. Schmitt. 2018. "Do Forelimb Shape and Peak Forces Co-Vary in Strepsirrhines?" *American Journal of Physical Anthropology* 167: 602–614. https://doi.org/10.1002/ajpa.23688.

Fabre, A. C., J. Marigó, M. C. Granatosky, and D. Schmitt. 2017. "Functional Associations Between Support Use and Forelimb Shape in Strepsirrhines and Their Relevance to Inferring Locomotor Behavior in Early Primates." *Journal of Human Evolution* 108: 11–30. https://doi.org/10.1016/j.jhevol.2017.03.012.

Fabre, A. C., L. Peckre, E. Pouydebat, and C. E. Wall. 2019. "Does the Shape of Forelimb Long Bones Co-Vary With Grasping Behaviour in Strepsirrhine Primates?" *Biological Journal of the Linnean Society* 127: 649–660. https://doi.org/10.1093/biolinnean/bly188.

Fleagle, J. G. 1980. "Locomotor Behavior of the Earliest Anthropoids: A Review of the Current Evidence." *Zeitschrift für Morphologie und Anthropologie* 71: 149–156.

Fleagle, J. G., and E. L. Simons. 1983. "The Tibio-Fibular Articulation in *Apidium phiomense*, an Oligocene Anthropoid." *Nature* 301: 238–239. https://doi.org/10.1038/301238a0.

Fleagle, J. G., and E. L. Simons. 1995. "Limb Skeleton and Locomotor Adaptations of *Apidium phiomense*, an Oligocene Anthropoid From Egypt." *American Journal of Physical Anthropology* 97: 235–289. https://doi.org/10.1002/ajpa.1330970303.

Friesen, S. E., R. P. Knigge, T. Jashashvili, W. E. Harcourt-Smith, M. J. Schoeninger, and M. W. Tocheri. 2024. "Shape Variation in the Talus

and Medial Cuneiform of Chimpanzees and Bonobos." *American Journal of Biological Anthropology* 183, no. 3: e24571. https://doi.org/10.1002/ajpa.24571.

Gebo, D. L. 1989. "Locomotor and Phylogenetic Considerations in Anthropoid Evolution." *Journal of Human Evolution* 18: 201–233. https://doi.org/10.1016/0047-2484(89)90050-X.

Gebo, D. L., K. C. Beard, M. F. Teaford, et al. 1988. "A Hominoid Proximal Humerus From the Early Miocene of Rusinga Island, Kenya." *Journal of Human Evolution* 17: 393–401. https://doi.org/10.1016/0047-2484(88)90028-0.

Gebo, D. L., N. R. Malit, and I. O. Nengo. 2009. "New Proconsuloid Postcranials From the Early Miocene of Kenya." *Primates* 50: 311–319. https://doi.org/10.1007/s10329-009-0151-4.

Gebo, D. L., and E. L. Simons. 1987. "Morphology and Locomotor Adaptations of the Foot in Early Oligocene Anthropoids." *American Journal of Physical Anthropology* 74: 83–101. https://doi.org/10.1002/ajpa.1330740108.

Gomberg, D. N. 1981. "Form and Function of the Hominoid Foot" (PhD diss., University of Massachusetts).

Hammond, A. S., D. M. Alba, S. Almécija, and S. Moyà-Solà. 2013. "Middle Miocene *Pierolapithecus* Provides a First Glimpse Into Early Hominid Pelvic Morphology." *Journal of Human Evolution* 64: 658–666. https://doi.org/10.1016/j.jhevol.2013.03.002.

Hammond, A. S., J. M. Plavcan, and C. V. Ward. 2016. "A Validated Method for Modeling Anthropoid Hip Abduction In Silico." *American Journal of Physical Anthropology* 160: 529–548. https://doi.org/10.1002/ajpa.22990.

Hammond, A. S., L. Rook, A. D. Anaya, et al. 2020. "Insights Into the Lower Torso in Late Miocene Hominoid *Oreopithecus bambolii*." *Proceedings of the National Academy of Sciences* 117: 278–284. https://doi.org/10.1073/pnas.1911896116.

Harrison, T. 1982. "Small-Bodied Apes From the Miocene of East Africa" (PhD diss., University College London).

Harrison, T. 1986. "A Reassessment of the Phylogenetic Relationships of *Oreopithecus bambolii* Gervais." *Journal of Human Evolution* 15: 541–583. https://doi.org/10.1016/S0047-2484(86)80073-2.

Hill, A., and S. Ward. 1988. "Origin of the Hominidae: The Record of African Large Hominoid Evolution Between 14 My and 4 My." *Yearbook of Physical Anthropology* 31: 49–83. https://doi.org/10.1002/ajpa.1330310505.

Hunt, K. D. 1991. "Positional Behavior in the Hominoidea." *International Journal of Primatology* 12: 95–118. https://doi.org/10.1007/BF02547576.

Hunt, K. D. 2016. "Why Are There Apes? Evidence for the Co-Evolution of Ape and Monkey Ecomorphology." *Journal of Anatomy* 228: 630–685. https://doi.org/10.1111/joa.12454.

Ishida, H., Y. Kunimatsu, T. Takano, Y. Nakano, and M. Nakatsukasa. 2004. "*Nacholapithecus* Skeleton From the Middle Miocene of Kenya." *Journal of Human Evolution* 46: 69–103. https://doi.org/10.1016/j.jhevol.2003.10.001.

Isler, K. 2002. "Characteristics of Vertical Climbing in African Apes." *Senckenbergiana Lethaea* 82: 115–124. https://doi.org/10.1007/BF03043777.

Jungers, W. L. 1987. "Body Size and Morphometric Affinities of the Appendicular Skeleton in *Oreopithecus bambolii* (IGF 11778)." *Journal of Human Evolution* 16: 445–456. https://doi.org/10.1016/0047-2484(87)90072-8.

Knigge, R. P., M. W. Tocheri, C. M. Orr, and K. P. Mcnulty. 2015. "Three-Dimensional Geometric Morphometric Analysis of Talar Morphology in Extant Gorilla Taxa From Highland and Lowland Habitats." *Anatomical Record* 298: 277–290. https://doi.org/10.1002/ar.23069.

Kordos, L., and D. R. Begun. 2001. "Primates From Rudabánya: Allocation of Specimens to Individuals, Sex and Age Categories." *Journal of Human Evolution* 40: 17–39. https://doi.org/10.1006/jhev.2000.0437.

Kuhn, M., and K. Johnson. 2013. *Applied Predictive Modeling.* Springer. https://doi.org/10.1007/978-1-4614-6849-3.

Langdon, J. H. 1986. *Functional Morphology of the Miocene Hominoid Foot.* Karger.

Larson, S. G. 1998. "Parallel Evolution in the Hominoid Trunk and Forelimb." *Evolutionary Anthropology* 6: 87–99. https://doi.org/10.1002/(SICI)1520-6505(1998)6:3%3C87::AID-EVAN3%3E3.0.CO;2-T.

Latimer, B., J. C. Ohman, and C. O. Lovejoy. 1987. "Talocrural Joint in African Hominoids: Implications for *Australopithecus afarensis.*" *American Journal of Physical Anthropology* 74: 155–175. https://doi.org/10.1002/ajpa.1330740204.

Le Gros Clark, W. E. 1952. "Report on Fossil Hominoid Material Collected by the British-Kenya Miocene Expedition, 1949-1951." *Proceedings of the Zoological Society of London* 122: 273–286. https://doi.org/10.1111/j.1096-3642.1952.tb00314.x.

Le Gros Clark, W. E., and L. S. B. Leakey. 1951. "The Miocene Hominoidea of East Africa." *Fossil Mammals of Africa* 1: 1–117.

Le Gros Clark, W. E., and D. P. Thomas. 1951. "Associated Jaws and Limb Bones of *Limnopithecus macinnesi.*" *Fossil Mammals of Africa* 3: 1–27.

Leakey, R. E. F., and M. G. Leakey. 1987. "A New Miocene Small-Bodied Ape From Kenya." *Journal of Human Evolution* 16, no. 4: 369–387. https://doi.org/10.1016/0047-2484(87)90067-4.

Leakey, R. E. F., M. G. Leakey, and A. C. Walker. 1988. "Morphology of *Afropithecus turkanensis* From Kenya." *American Journal of Physical Anthropology* 76, no. 3: 289–307. https://doi.org/10.1002/ajpa.1330760303.

Leardini, A., J. J. O'Connor, F. Catani, and S. Giannini. 2000. "The Role of the Passive Structures in the Mobility and Stability of the Human Ankle Joint: A Literature Review." *Foot & Ankle* 21: 602–615. https://doi.org/10.1177/107110070002100715.

Lewis, O. J. 1980a. "The Joints of the Evolving Foot. Part I. The Ankle Joint." *Journal of Anatomy* 130: 527–543.

Lewis, O. J. 1980b. "The Joints of the Evolving Foot. Part II. The Intrinsic Joints." *Journal of Anatomy* 130: 833–857.

Lisowski, F. P., G. H. Albrecht, and C. E. Oxnard. 1974. "The Form of the Talus in Some Higher Primates: A Multivariate Study." *American Journal of Physical Anthropology* 41: 191–215. https://doi.org/10.1002/ajpa.1330410203.

Lisowski, F. P., G. H. Albrecht, and C. E. Oxnard. 1976. "African Fossil Tali: Further Multivariate Morphometric Studies." *American Journal of Physical Anthropology* 45: 5–18. https://doi.org/10.1002/ajpa.1330450103.

Llera Martín, C. J., K. D. Rose, and A. D. Sylvester. 2022. "A Morphometric Analysis of Early Eocene Euprimate Tarsals From Gujarat, India." *Journal of Human Evolution* 164: 103141. https://doi.org/10.1016/j.jhevol.2022.103141.

MacInnes, C. 1943. "Notes on the East African Miocene Primates." *Journal of the East African Uganda Natural History Society* 17: 141–181.

Madar, S. I. 1996. "The Postcranial Morphology of *Sivapithecus*, an Asian Large-Bodied Miocene Hominoid" (PhD diss., Kent State University).

Manduell, K. L., H. C. Morrogh-Bernard, and S. K. Thorpe. 2011. "Locomotor Behavior of Wild Orangutans (*Pongo pygmaeus wurmbii*) in Disturbed Peat Swamp Forest, Sabangau, Central Kalimantan, Indonesia." *American Journal of Physical Anthropology* 145: 348–359. https://doi.org/10.1002/ajpa.21495.

Marigó, J., I. Roig, E. R. Seiffert, S. Moyà-Solà, and D. M. Boyer. 2016. "Astragalar and Calcaneal Morphology of the Middle Eocene Primate *Anchomomys frontanyensis* (Anchomomyini): Implications for Early Primate Evolution." *Journal of Human Evolution* 91: 122–143. https://doi.org/10.1016/j.jhevol.2015.08.011.

McCrossin, M. 1994. "The Phylogenetic Relationships, Adaptations, and Ecology of *Kenyapithecus*" (PhD diss., University of California Berkeley).

Meldrum, D. J., and R. E. Wunderlich. 1998. "Midfoot Flexibility in Ape Foot Dynamics, Early Hominid Footprints, and Bipedalism." *American Journal of Physical Anthropology* 105, no. S26: 161. https://doi.org/10.1002/(SICI)1096-8644(1998)26+%3C100::AID-AJPA8%3E3.0.CO;2-7.

Monclús-Gonzalo, O., D. M. Alba, A. Duhamel, A. C. Fabre, and J. Marigó. 2023. "Early Euprimates Already Had a Diverse Locomotor Repertoire: Evidence From Ankle Bone Morphology." *Journal of Human Evolution* 181: 103395. https://doi.org/10.1016/j.jhevol.2023.103395.

Morbeck, M. E. 1983. "Miocene Hominoid Discoveries From Rudabánya: Implications From the Postcranial Skeleton." In *New Interpretations of Ape and Human Ancestry*, edited by R. L. Ciochon and R. S. Corruccini, 369–404. Plenum Press. https://doi.org/10.1007/978-1-4684-8854-8_14.

Moyà-Solà, S., D. M. Alba, S. Almécija, et al. 2009. "A Unique Middle Miocene European Hominoid and the Origins of the Great Ape and Human Clade." *Proceedings of the National Academy of Sciences* 106: 9601–9606. https://doi.org/10.1073/pnas.0811730106.

Moyà-Solà, S., and M. Köhler. 1993. "Recent Discoveries of *Dryopithecus* Shed New Light on Evolution of Great Apes." *Nature* 365, no. 6446: 543–545. https://doi.org/10.1038/365543a0.

Moyà-Solà, S., and M. Köhler. 1995. "New Partial Cranium of *Dryopithecus* Lartet, 1863 (Hominoidea, Primates) From the Upper Miocene of Can Llobateres, Barcelona, Spain." *Journal of Human Evolution* 29, no. 2: 101–139. https://doi.org/10.1006/jhev.1995.1049.

Moyà-Solà, S., and M. Köhler. 1996. "A *Dryopithecus* Skeleton and the Origins of Great-Ape Locomotion." *Nature* 379: 156–159. https://doi.org/10.1038/379156a0.

Moyà-Solà, S., M. Köhler, D. M. Alba, I. Casanovas-Vilar, and J. Galindo. 2004. "*Pierolapithecus catalaunicus*, a New Middle Miocene Great Ape From Spain." *Science* 306: 1339–1344. https://doi.org/10.1126/science.1103094.

Moyà-Solà, S., M. Köhler, D. M. Alba, I. Casanovas-Vilar, and J. Galindo. 2005. "Response to Comment on 'Pierolapithecus catalaunicus, a New Middle Miocene Great Ape From Spain'." *Science* 308: 203d. https://doi.org/10.1126/science.1108433.

Moyà-Solà, S., M. Köhler, D. M. Alba, et al. 2009. "First Partial Face and Upper Dentition of the Middle Miocene Hominoid *Dryopithecus Fontani* From Abocador de Can Mata (Vallès-Penedès Basin, Catalonia, NE Spain): Taxonomic and Phylogenetic Implications." *American Journal of Physical Anthropology* 139: 126–145. https://doi.org/10.1002/ajpa.20891.

Nakatsukasa, M., Y. Kunimatsu, D. Shimizu, Y. Nakano, Y. Kikuchi, and H. Ishida. 2012. "Hind Limb of the *Nacholapithecus kerioi* Holotype and Implications for Its Positional Behavior." *Anthropological Science* 120, no. 3: 235–250. https://doi.org/10.1537/ase.120731.

Parr, W. C. H., H. J. Chatterjee, and C. Soligo. 2011. "Inter- and Intra-Specific Scaling of Articular Surface Areas in the Hominoid Talus." *Journal of Anatomy* 218: 386–401. https://doi.org/10.1111/j.1469-7580.2011.01347.x.

Parr, W. C. H., C. Soligo, J. Smaers, et al. 2014. "Three-Dimensional Shape Variation of Talar Surface Morphology in Hominoid Primates." *Journal of Anatomy* 225: 42–59. https://doi.org/10.1111/joa.12195.

Pilbeam, D. R., G. E. Meyer, C. Badgley, et al. 1977. "New Hominoid Primates From the Siwaliks of Pakistan and Their Bearing on Hominoid Evolution." *Nature* 270, no. 5639: 689–695. https://doi.org/10.1038/270689a0.

Pilbeam, D. R., M. D. Rose, C. Badgley, and B. Lipschutz. 1980. "Miocene Hominoids From Pakistan." *Postilla* 181: 1–94.

Pina, M., D. M. Alba, S. Moyà-Solà, and S. Almécija. 2019. "Femoral Neck Cortical Bone Distribution of Dryopithecin Apes and the Evolution of Hominid Locomotion." *Journal of Human Evolution* 136: 102651. https://doi.org/10.1016/j.jhevol.2019.102651.

Pina, M., S. Almécija, D. M. Alba, M. C. O'Neil, and S. Moyà-Solà. 2014. "The Middle Miocene Ape *Pierolapithecus catalaunicus* Exhibits Extant Great Ape-Like Morphometric Affinities on Its Patella: Inferences on Knee Function and Evolution." *PLoS One* 9: e91944. https://doi.org/10.1371/journal.pone.0091944.

Pina, M., D. DeMiguel, F. Puigvert, J. Marcé-Nogué, and S. Moyà-Solà. 2020. "Knee Function Through Finite Element Analysis and the Role of Miocene Hominoids in Our Understanding of the Origin of Antipronograde Behaviours: The *Pierolapithecus catalaunicus* Patella as a Case Study." *Palaeontology* 63, no. 3: 459–475. https://doi.org/10.1111/pala.12466.

Pugh, K. D. 2022. "Phylogenetic Analysis of Middle-Late Miocene Apes." *Journal of Human Evolution* 165: 103140. https://doi.org/10.1016/j.jhevol.2021.103140.

Pugh, K. D., S. A. Catalano, M. Pérez de los Ríos, et al. 2023. "The Reconstructed Cranium of *Pierolapithecus* and the Evolution of the Great Ape Face." *Proceedings of the National Academy of Sciences* 120: e2218778120. https://doi.org/10.1073/pnas.2218778120.

Püschel, T. A., J. T. Gladman, R. Bobe, and W. I. Sellers. 2017. "The Evolution of the Platyrrhine Talus: A Comparative Analysis of the Phenetic Affinities of the Miocene Platyrrhines With Their Modern Relatives." *Journal of Human Evolution* 111: 179–201. https://doi.org/10.1016/j.jhevol.2017.07.015.

Püschel, T. A., J. Marcé-Nogué, J. Gladman, B. A. Patel, S. Almécija, and W. I. Sellers. 2020. "Getting Its Feet on the Ground: Elucidating *Paralouatta*'s Semi-Terrestriality Using the Virtual Morpho-Functional Toolbox." *Frontiers in Earth Science* 8: 79. https://doi.org/10.3389/feart.2020.00079.

Püschel, T. A., J. Marcé-Nogué, J. T. Gladman, R. Bobe, and W. I. Sellers. 2018. "Inferring Locomotor Behaviours in Miocene New World Monkeys Using Finite Element Analysis, Geometric Morphometrics, and Machine-Learning Classification Techniques Applied to Talar Morphology." *Journal of the Royal Society Interface* 15, no. 146: 20180520. https://doi.org/10.1098/rsif.2018.0520.

R Core Team. 2024. *R: A Language and Environment for Statistical Computing.* R Foundation for Statistical Computing.

Rafferty, K. L., A. Walker, C. B. Ruff, M. D. Rose, and P. J. Andrews. 1995. "Postcranial Estimates of Body Weight in Proconsul, With a Note on a Distal Tibia of *P. major* From Napak, Uganda." *American Journal of Physical Anthropology* 97: 391–402. https://doi.org/10.1002/ajpa.1330970406.

Raffi, I., B. S. Wade, H. Pälike, et al. 2020. "The Neogene Period." In *Geologic Time Scale 2020*, edited by F. M. Gradstein, J. G. Ogg, M. D. Schmitz, and G. M. Ogg, 1141–1215. Elsevier. https://doi.org/10.1016/B978-0-12-824360-2.00029-2.

Ramos, G. L., III. 2014. "Positional Behavior of *Pan paniscus* at Lui Kotale, Democratic Republic of Congo" (PhD diss., Indiana University).

Rohlf, F. J. 2021. "Why Clusters and Other Patterns Can Seem to Be Found in Analyses of High-Dimensional Data." *Evolutionary Biology* 48: 1–16. https://doi.org/10.1007/s11692-020-09518-6.

Rohlf, F. J., and M. Corti. 2000. "Use of Two-Block Partial Least-Squares to Study Covariation in Shape." *Systematic Biology* 49: 740–753. https://doi.org/10.1080/106351500750049806.

Rosas, A., A. Ferrando, M. Bastir, et al. 2017. "Neandertal Talus Bones From El Sidrón Site (Asturias, Spain): A 3D Geometric Morphometrics Analysis." *American Journal of Physical Anthropology* 164: 394–415. https://doi.org/10.1002/ajpa.23280.

Rose, M. D. 1983. "Miocene Hominoid Postcranial Morphology. Monkey-Like, Ape-Like, Neither, or Both?" In *New Interpretations of Ape and Human Ancestry*, edited by R. L. Ciochon and R. S. Corruccini, 503–516. Plenum Press. https://doi.org/10.1007/978-1-4684-8854-8_15.

Rose, M. D. 1988. "Another Look at the Anthropoid Elbow." *Journal of Human Evolution* 17: 193–224. https://doi.org/10.1016/0047-2484(88)90054-1.

Rose, M. D. 1994. "Quadrupedalism in Some Miocene Catarrhines." *Journal of Human Evolution* 26: 387–411. https://doi.org/10.1006/jhev.1994.1025.

Rose, M. D., M. G. Leakey, R. E. F. Leakey, and A. C. Walker. 1992. "Postcranial Specimens of *Simiolus enjiessi* and Other Primitive Catarrhines From the Early Miocene of Lake Turkana, Kenya." *Journal of Human Evolution* 22, no. 3: 171–237. https://doi.org/10.1016/S0047-2484(05)80006-5.

Rose, M. D., Y. Nakano, and H. Ishida. 1996. "*Kenyapithecus* Postcranial Specimens From Nachola, Kenya." *African Studies Monographs Supplement* 24: 3–56. https://doi.org/10.14989/68384.

Russo, G. A., T. C. Prang, F. R. McGechie, et al. 2024. "An Ape Partial Postcranial Skeleton (KNM-NP 64631) From the Middle Miocene of Napudet, Northern Kenya." *Journal of Human Evolution* 192: 103519. https://doi.org/10.1016/j.jhevol.2024.103519.

Russo, G. A., and L. J. Shapiro. 2013. "Reevaluation of the Lumbosacral Region of *Oreopithecus bambolii*." *Journal of Human Evolution* 65: 253–265. https://doi.org/10.1016/j.jhevol.2013.05.004.

Sarmiento, E. E. 1983. "The Significance of the Heel Process in Anthropoids." *International Journal of Primatology* 4: 127–152. https://doi.org/10.1007/BF02743754.

Schlager, S. 2013. "Soft-Tissue Reconstruction of the Human Nose: Population Differences and Sexual Dimorphism" (PhD diss., Albert-Ludwigs-Universität Freiburg).

Schlager, S. 2017. "Morpho and Rvcg–Shape Analysis in R: R-Packages for Geometric Morphometrics, Shape Analysis and Surface Manipulations." In *Statistical Shape and Deformation Analysis: Methods, Implementation and Applications*, edited by G. Zheng, S. Li, and G. Székely, 217–256. Academic Press. https://doi.org/10.1016/B978-0-12-810493-4.00011-0.

Schön Ybarra, M. A., and M. A. Schön III. 1987. "Positional Behavior and Limb Bone Adaptations in Red Howling Monkeys (*Alouatta seniculus*)." *Folia Primatologica* 49: 70–89. https://doi.org/10.1159/000156310.

Schrein, C. M. 2006. "Metric Variation and Sexual Dimorphism in the Dentition of *Ouranopithecus macedoniensis*." *Journal of Human Evolution* 50: 460–468. https://doi.org/10.1016/j.jhevol.2005.11.007.

Scott, J. E., C. M. Schrein, and J. Kelley. 2009. "Beyond *Gorilla* and *Pongo*: Alternative Models for Evaluating Variation and Sexual Dimorphism in Fossil Hominoid Samples." *American Journal of Physical Anthropology* 140: 253–264. https://doi.org/10.1002/ajpa.21059.

Seiffert, E. R., and E. L. Simons. 2001. "Astragalar Morphology of Late Eocene Anthropoids From the Fayum Depression (Egypt) and the Origin of Catarrhine Primates." *Journal of Human Evolution* 41: 577–606. https://doi.org/10.1006/jhev.2001.0508.

Senut, B. 2012. "Les Restes Post-Crâniens des Pliopithecidae (Primates) de Sansan." *Mémoires du Muséum National D'histoire Naturelle* 203: 535–558.

Shearer, B. M., S. B. Cooke, L. B. Halenar, et al. 2017. "Evaluating Causes of Error in Landmark-Based Data Collection Using Scanners." *PLoS One* 12: e0187452.

Smith, R. J. 1993. "Bias in Equations Used to Estimate Fossil Primate Body Mass." *Journal of Human Evolution* 25: 31–41. https://doi.org/10.1006/jhev.1993.1036.

Smith, R. J., and W. L. Jungers. 1997. "Body Mass in Comparative Primatology." *Journal of Human Evolution* 32: 523–559. https://doi.org/10.1006/jhev.1996.0122.

Sorrentino, R., K. J. Carlson, E. Bortolini, et al. 2020. "Morphometric Analysis of the Hominin Talus: Evolutionary and Functional Implications." *Journal of Human Evolution* 142: 102747. https://doi.org/10.1016/j.jhevol.2020.102747.

Strasser, E. 1988. "Pedal Evidence for the Origin and Diversification of Cercopithecid Clades." *Journal of Human Evolution* 17: 225–245. https://doi.org/10.1016/0047-2484(88)90055-3.

Straus, W. L. 1963. "The Classification of *Oreopithecus*." In *Classification and Human Evolution*, edited by S. L. Washburn, 146–177. Routledge.

Susanna, I., D. M. Alba, S. Almécija, and S. Moyà-Solà. 2014. "The Vertebral Remains of the Late Miocene Great Ape *Hispanopithecus laietanus* From Can Llobateres 2 (Vallès-Penedès Basin, NE Iberian Peninsula)." *Journal of Human Evolution* 73: 15–34. https://doi.org/10.1016/j.jhevol.2014.05.009.

Szalay, F. S., and J. H. Langdon. 1986. "The Foot of *Oreopithecus*: An Evolutionary Assessment." *Journal of Human Evolution* 15: 585–621. https://doi.org/10.1016/S0047-2484(86)80074-4.

Tallman, M., S. Almécija, S. L. Reber, D. M. Alba, and S. Moyà-Solà. 2013. "The Distal Tibia of *Hispanopithecus laietanus*: More Evidence for Mosaic Evolution in Miocene Apes." *Journal of Human Evolution* 64: 319–327. https://doi.org/10.1016/j.jhevol.2012.07.009.

Tocheri, M. W., C. R. Solhan, C. M. Orr, et al. 2011. "Ecological Divergence and Medial Cuneiform Morphology in Gorillas." *Journal of Human Evolution* 60: 171–184. https://doi.org/10.1016/j.jhevol.2010.09.002.

Torres-Tamayo, N., S. Schlager, D. García-Martínez, et al. 2020. "Three-Dimensional Geometric Morphometrics of Thorax-Pelvis Covariation and Its Potential for Predicting the Thorax Morphology: A Case Study on Kebara 2 Neandertal." *Journal of Human Evolution* 147: 102854. https://doi.org/10.1016/j.jhevol.2020.102854.

Tsubamoto, T., N. Egi, M. Takai, Thaung-Htike, and Zin-Maung-Maung-Thein. 2016. "Body Mass Estimation From the Talus in Primates and Its Application to the Pondaung Fossil Amphipithecid Primates." *Historical Biology* 28: 27–34. https://doi.org/10.1080/08912963.2014.971783.

Turley, K., and S. R. Frost. 2013. "The Shape and Presentation of the Catarrhine Talus: A Geometric Morphometric Analysis." *Anatomical Record* 296: 877–890. https://doi.org/10.1002/ar.22696.

Tuttle, R. 1975. "Parallelism, Brachiation, and Hominoid Phylogeny." In *Phylogeny of the Primates*, edited by W. P. Luckett and F. S. Szalay, 447–480. Plenum Press. https://doi.org/10.1007/978-1-4684-2166-8_17.

Urciuoli, A., and D. M. Alba. 2023. "Systematics of Miocene Apes: State of the Art of a Neverending Controversy." *Journal of Human Evolution* 175: 103309. https://doi.org/10.1016/j.jhevol.2022.103309.

Urciuoli, A., C. Zanolli, S. Almécija, et al. 2021. "Reassessment of the Phylogenetic Relationships of the Late Miocene Apes *Hispanopithecus* and *Rudapithecus* Based on Vestibular Morphology." *Proceedings of the National Academy of Sciences of the United States of America* 118, no. 5: e2015215118. https://doi.org/10.1073/pnas.2015215118.

Vereecke, E. E., K. D'Août, R. Payne, and P. Aerts. 2005. "Functional Analysis of the Foot and Ankle Myology of Gibbons and Bonobos." *Journal of Anatomy* 206: 453–476. https://doi.org/10.1111/j.1469-7580.2005.00412.x.

Walker, A. 1997. "Proconsul. Function and Phylogeny." In *Function, Phylogeny and Fossils: Miocene Hominoid Evolution and Adaptation*, edited by D. R. Begun, C. V. Ward, and M. D. Rose, 209–224. Plenum Press. https://doi.org/10.1007/978-1-4899-0075-3_10.

Walker, A., and M. Pickford. 1983. "New Postcranial Fossils of *Proconsul africanus* and *Proconsul nyanzae*." In *New Interpretations of Ape and Human Ancestry*, edited by R. L. Ciochon and R. S. Corruccini, 325–351. Plenum Press. https://doi.org/10.1007/978-1-4684-8854-8_12.

Ward, C. V. 1993. "Torso Morphology and Locomotion in *Proconsul nyanzae*." *American Journal of Physical Anthropology* 92: 291–328. https://doi.org/10.1002/ajpa.1330920306.

Ward, C. V. 1997. "Functional Anatomy and Phyletic Implications of the Hominoid Trunk and Hindlimb." In *Function, Phylogeny and Fossils: Miocene Hominoid Evolution and Adaptation*, edited by D. R. Begun, C. V. Ward, and M. D. Rose, 101–130. Plenum Press. https://doi.org/10.1007/978-1-4899-0075-3_6.

Ward, C. V. 1998. "*Afropithecus*, *Proconsul*, and the Primitive Hominoid Skeleton." In *Primate Locomotion*, edited by E. Strasser, J. G. Fleagle, A. L. Rosenberger, and H. M. McHenry, 337–352. Plenum Press. https://doi.org/10.1007/978-1-4899-0092-0_18.

Ward, C. V. 2015. "Postcranial and Locomotor Adaptations of Hominoids." In *Handbook of Paleoanthropology*, edited by W. Henke and I. Tattersall, 2nd ed., 1363–1386. Springer Berlin Heidelberg. https://doi.org/10.1007/978-3-642-39979-4_34.

Ward, C. V., C. B. Ruff, A. Walker, M. F. Teaford, M. D. Rose, and I. O. Nengo. 1995. "Functional Morphology of *Proconsul* Patellas From Rusinga Island, Kenya, With Implications for Other Miocene-Pliocene Catarrhines." *Journal of Human Evolution* 29: 1–19. https://doi.org/10.1006/jhev.1995.1045.

Ward, C. V., A. Walker, M. F. Teaford, and I. Odhiambo. 1993. "Partial Skeleton of *Proconsul nyanzae* From Mfangano Island, Kenya." *American Journal of Physical Anthropology* 90: 77–111. https://doi.org/10.1002/ajpa.1330900106.

Wickham, H. 2016. *ggplot2: Elegant Graphics for Data Analysis*. Springer.

Wiley, D. F., N. Amenta, D. A. Alcantara, et al. 2005. "Evolutionary Morphing." In *VIS 05: IEEE Visualization 2005*, edited by C. T. Silva, E. Gröller, and H. E. Rushmeier, 431–438. Institute of Electrical and Electronics Engineers. https://doi.org/10.1109/VISUAL.2005.1532826.

Willmott, C. J., and K. Matsuura. 2005. "Advantages of the Mean Absolute Error (MAE) Over the Root Mean Square Error (RMSE) in Assessing Average Model Performance." *Climate Research* 30: 79–82. https://doi.org/10.3354/cr030079.

Wold, S., M. Sjöström, and L. Eriksson. 2001. "PLS-Regression: A Basic Tool of Chemometrics." *Chemometrics and Intelligent Laboratory Systems* 58, no. 2: 109–130. https://doi.org/10.1016/S0169-7439(01)00155-1.

Yapuncich, G. S., J. T. Gladman, and D. M. Boyer. 2015. "Predicting Euarchontan Body Mass: A Comparison of Tarsal and Dental Variables." *American Journal of Physical Anthropology* 157: 472–506. https://doi.org/10.1002/ajpa.22735.

Yapuncich, G. S., and M. C. Granatosky. 2021. "Footloose: Articular Surface Morphology and Joint Movement Potential in the Ankles of Lorisids and Cheirogaleids." *American Journal of Physical Anthropology* 175: 876–894. https://doi.org/10.1002/ajpa.24298.

Youlatos, D. 1999. "Étude Fonctionnelle Multivariée de l'Astragale et du Calcanéum de *Mesopithecus pentelici*, Wagner, 1839 (Cercopithecoidea, Primates)." *Primatologie* 2: 407–420.

Youlatos, D., and J. Meldrum. 2011. "Locomotor Diversification in New World Monkeys: Running, Climbing, or Clawing Along Evolutionary

Branches." *Anatomical Record* 294: 1991–2012. https://doi.org/10.1002/ar.21508.

Zapfe, H. 1958. "The Skeleton of *Pliopithecus* (*Epipliopithecus*) *vindobonensis* Zapfe and Hürzeler." *American Journal of Physical Anthropology* 16: 441–457. https://doi.org/10.1002/ajpa.1330160405.

Zelditch, M. L., D. L. Swiderski, and H. D. Sheets. 2012. *Geometric Morphometrics for Biologists. A Primer.* 2nd ed. Academic Press.

Supporting Information

Additional supporting information can be found online in the Supporting Information section.